

## Personalized Itinerary Planner and Abstract Book

AGU 2011 Fall Meeting  
December 04 - 09, 2011

To make changes to your itinerary or view the full meeting schedule, visit <http://agu-fm11.abstractcentral.com:80>

Powered By



THOMSON REUTERS

Sunday, December 04, 2011

*You have nothing scheduled for this day*

Monday, December 05, 2011

Time	Session Info
8:00 AM-10:00 AM, Room 2012 (Moscone West), <b>T11D. Linking Plate Tectonic and Surface Processes to the Deep Earth I</b>	
8:00-8:15 AM	<b>T11D-01. Coupling Climate, Surface Processes and Mantle Convection (<i>Invited</i>)</b> <u>R. Moucha</u> ; J. Braun; A.M. Forte; A.B. Bush; D.B. Rowley; F. Guillocheau; C. Robin
1:40 PM-6:00 PM, Halls A-C (Moscone South), <b>U13A. The Early Earth: Emergence of a Habitable Planet II Posters</b>	
1:40 PM-6:00 PM	<b>U13A-0029. Geochemical and petrological study of Barberton Greenstone Belt cherts (3.2-3.5 Ga), South Africa</b> <u>M. Ledevin</u> ; N. Arndt; A. Simionovici
1:40 PM-6:00 PM, Halls A-C (Moscone South), <b>H13A. Characterization of Fault Zone Hydrology III Posters</b>	
1:40 PM-6:00 PM	<b>H13A-1188. Reservoir-Seal-Fault Systems Leakage Evolution Though Time and Space</b> <u>E. Frery</u> ; N. Ellouz; J. Gratier; P. Deschamps
1:40 PM-6:00 PM, Halls A-C (Moscone South), <b>T13E. Properties and Physics of Fault Zone Damage III Posters</b>	
1:40 PM-6:00 PM	<b>T13E-2431. Origin of fault roughness and the development of slip surfaces</b> <u>T. Candela</u> ; F. Renard
4:00 PM-6:00 PM, Room 3024 (Moscone West), <b>G14A. Plate Motion and Continental Tectonics III</b>	
5:30-5:45 PM	<b>G14A-07. Interseismic coupling and block motion along the northern Peru and southern Ecuador subduction zone (<i>Invited</i>)</b> <u>F. Rolandone</u> ; J. Nocquet; J. Villegas Lanza; P.A. Mothes; D. Cisneros Revelo ; M. Chlieh ; L. Audin; H. Tavera; P. Jarrin ; E.O. Norabuena; F. Bondoux

Tuesday, December 06, 2011

Time	Session Info
8:00 AM-10:00 AM, Room 2009 (Moscone West), <b>S21D. The Static Versus Dynamic Earthquake Triggering Debate: What's New and What's Next? II</b>	

8:45-9:00 AM	<b>S21D-04. INVESTIGATING TRIGGERING IN SEISMICITY PATTERNS; THE SPECIAL CASE OF TRIGGERING DISTANCE DISTRIBUTIONS</b> ( <i>Invited</i> ) <u>D. Marsan</u>
10:20 AM-12:20 PM, Room 2009 (Moscone West), <b>S22B. The Static Versus Dynamic Earthquake Triggering Debate: What's New and What's Next? III</b>	
11:50-12:05 PM	<b>S22B-07. Link between Coulomb stress changes and seismic activation in the Marmara sea after the Izmit (Turkey) earthquake</b> <u>V. Durand</u> ; M.P. Bouchon; H. Karabulut; J. Schmittbuhl; D. Marsan
1:40 PM-6:00 PM, Halls A-C (Moscone South), <b>G23A. InSAR Applications for the Detection of Crustal Deformation III Posters</b>	
1:40 PM-6:00 PM	<b>G23A-0841. The 2009-2010 Guerrero Slow Slip Event Monitored by InSAR, Using Time Series Approach.</b> <u>G. Bacques</u> ; E. Pathier; C. Lasserre; F. Cotton; M. Radiguet
1:40 PM-6:00 PM, Halls A-C (Moscone South), <b>S23A. Advances in Signal Processing Methods for Seismology I Posters</b>	
1:40 PM-6:00 PM	<b>S23A-2230. Comparison between two methods for forward calculation of ambient noise H/V spectral ratios</b> <u>A. Garcia-Jerez</u> ; F. Luzón; F.J. Sanchez-Sesma; M.A. Santoyo; D. Albarello; E. Lunedei; M. Campillo; U. Iturrarán-Viveros
1:40 PM-6:00 PM, Halls A-C (Moscone South), <b>S23B. Observations and Modeling of Tremor and Slow Slip and Implications for Plate Boundaries I Posters</b>	
1:40 PM-6:00 PM	<b>S23B-2263. Temporal variations of non-volcanic tremor (NVT) locations in the Mexican subduction zone: finding the NVT sweet spot</b> <u>A.L. Husker</u> ; V. Kostoglodov; V.M. Cruz-Atienza; D. Legrand; N.M. Shapiro; J.S. Payero; M. Campillo; E. Huesca-Perez
1:40-1:40 PM	<b>S23B-2264. Toward a Unified Theory of Silent Seismicity in Central Mexico</b> <u>V.M. Cruz-Atienza</u> ; D.N. Rivet; V. Kostoglodov; A.L. Husker; D. Legrand; M. Campillo
1:40-1:40 PM	<b>S23B-2279. Tectonic Tremor analysis with the Taiwan Chelungpu-Fault Drilling Program (TCDP) downhole seismometer array</b> <u>Y. Lin</u> ; G. Hillers; K. Ma; M. Campillo
1:40 PM-6:00 PM, Halls A-C (Moscone South), <b>T23C. Mechanics of the Lithospheric Deformation During the Earthquake Cycle I Posters</b>	
1:40 PM-6:00 PM	<b>T23C-2412. Spatial and temporal evolution of aseismic slip along the Haiyuan fault from SAR interferometry</b> <u>R. Jolivet</u> ; C. Lasserre; T. Candela; F. Renard; M. Doin; G. Peltzer
1:40 PM-6:00 PM, Halls A-C (Moscone South), <b>T23E. What Can Fault Rocks Tell Us About Earthquake Mechanics? I Posters</b>	

1:40 PM-6:00 PM	<b>T23E-2462. The evolution of fabric with displacement in natural brittle faults</b>  <u>S. Mitterpergher</u> ; G. Di Toro; J. Gratier; S. Aretusini; A. Boullier-Bertrand
1:40 PM-3:40 PM, Room 304 (Moscone South), <b>GP23B. Models and Observations of the Geomagnetic Field Including Dynamo Studies I</b>	
2:25-2:40 PM	<b>GP23B-04. Zonal shear and super-rotation in a magnetized spherical Couette flow experiment</b> <u>D. Brito</u> ; T. Alboussière; P. CARDIN; N. Gagnière; D. Jault; P. La Rizza; J. Masson; H. Nataf; D. Schmitt
4:00 PM-6:00 PM, Room 2009 (Moscone West), <b>S24A. Monitoring Temporal Changes of Earth's Properties with Seismic Waves II</b>	
4:30-5:00 PM <a href="#">(Conflict)</a>	<b>S24A-03. Observations of non-linear behavior of seismic speed at low strain rate (<i>Invited</i>)</b> <u>M. Campillo</u> ; L. Retailleau; D.N. Rivet; G. Hillers; L.A. Rivera; T. Nishimura; K. Ma
4:00 PM-5:00 PM, Room 304 (Moscone South), <b>GP24B. Models and Observations of the Geomagnetic Field including Dynamo Studies II</b>	
4:45-5:00 PM <a href="#">(Conflict)</a>	<b>GP24B-04. reconstructing the geomagnetic field over the observatory era with a Bayesian approach (<i>Invited</i>)</b> <u>N. Gillet</u> ; D. Jault; C.C. Finlay
4:00 PM-6:00 PM, Room 2009 (Moscone West), <b>S24A. Monitoring Temporal Changes of Earth's Properties with Seismic Waves II</b>	
5:30-5:45 PM	<b>S24A-06. Locating a small change in a multiple scattering environment.</b> <u>T. Planes</u> ; E.F. Larose; V. Rossetto; L. Margerin
5:45-6:00 PM	<b>S24A-07. Using Diffuse Field Theory to Interpret the H/V Spectral Ratio from Earthquake Records in a Mexico City site</b> <u>V. Salinas</u> ; F. Luzón; F.J. Sanchez-Sesma; H. Kawase; S. Matsushima; M. Suárez; A. Cuéllar; D.N. Rivet; M. Campillo

Wednesday, December 07, 2011

Time	Session Info
8:00 AM-12:20 PM, Halls A-C (Moscone South), <b>A31A. Advances in Atmospheric Infrasound I Posters</b>	
8:00 AM-12:20 PM	<b>A31A-0043. Studying of Infrasonic Sources Generated by the Swell</b> <u>M. Landès</u> ; L. Ceranna; A. LE PICHON; G. Hillers; R.S. Matoza
8:00 AM-12:20 PM, Halls A-C (Moscone South), <b>ED31A. Education General Contributions I Posters</b>	

8:00 AM-12:20 PM	<b>ED31A-0727. THE LITHOSPHERIC STRUCTURE OF THE WESTERN TURKEY AND AEGEAN REGION</b> <u>T. Afacan Ergun</u> ; H. Karabulut; A. Paul
8:00 AM-12:20 PM, Halls A-C (Moscone South), <b>EP31E. The Physics of Granular and Turbulent Flows in Geomorphology III Posters</b>	
8:00 AM-12:20 PM	<b>EP31E-0863. Scaling Analysis of Deformation Field within Granular Materials: application to Strain Localization.</b> D. Amitrano; <u>F. Gimbert</u> ; G. Combe; J. Weiss
8:00 AM-12:20 PM, Halls A-C (Moscone South), <b>H31D. Recent Advances in Hydrogeology: Innovative Solutions to Single and Multiphase Flow and Transport Issues I Posters</b>	
8:00 AM-12:20 PM	<b>H31D-1194. Experimental lighting of water velocity around macropores in a porous media</b> <u>L. Lassabatere</u> ; T. Lenoir; P. Peyneau; E. Lamy; B. Bechet; R. Angulo-Jaramillo; A. Simionovici; A. Manceau
8:00 AM-12:20 PM, Halls A-C (Moscone South), <b>S31C. Monitoring Temporal Changes of Earth's Properties with Seismic Waves III Posters</b>	
8:00 AM-12:20 PM	<b>S31C-2251. Do variations of the ambient noise wavefield reflect on measured seismic velocity changes?</b> <u>C. Hadziioannou</u> ; E.F. Larose; P. Roux; M. Campillo; J.M. Wassermann; H. Igel
8:00-8:00 AM	<b>S31C-2259. Using curvelet filter to improve the temporal resolution of seismic waves speed changes measured from ambient noise correlations.</b> <u>L. Stehly</u> ; B. FROMENT; M. Campillo; J. Chen; Q. Liu
8:00 AM-10:00 AM, Room 2018 (Moscone West), <b>V31H. Magmatic Plumbing Systems I</b>	
8:45-9:00 AM	<b>V31H-04. Deformation cycle of the Grímsvötn sub-glacial volcano, Iceland, measured by GPS</b> <u>E.C. Sturkell</u> ; F. Sigmundsson; P. Einarsson; S. Hreinsdottir; T. Villemin; H. Geirsson; B.G. Ófeigsson; F. Jouanne; H. Bjornsson; G.B. Gudmundsson; F. Pálsson
8:00 AM-10:00 AM, Room 2007 (Moscone West), <b>S31G. Observations and Modeling of Tremor and Slow Slip and Implications for Plate Boundaries II</b>	
9:30-9:45 AM	<b>S31G-07. Slow slip events and strain accumulation in the Guerrero gap, Mexico.</b> M. Radiguet; <u>F. Cotton</u> ; M.M. Vergnolle; M. Campillo; A. Walpersdorf; N. Cotte; V. Kostoglodov
9:45-10:00 AM	<b>S31G-08. New Results of Studies of Slow Slip Events and Nonvolcanic Tremor in the Guerrero Seismic Gap, Mexico (G-GAP project)</b> <u>V. Kostoglodov</u> ; D. Zigone; A.L. Husker; M. Campillo; D.N. Rivet; N.M. Shapiro; M. Radiguet; W. Frank; G. Hillers; N. Cotte; G. Cougoulat; J.S. Payero; V. Cruz-Atienza
1:40 PM-6:00 PM, Halls A-C (Moscone South), <b>NS33A. From Pore-Scale to Basin-Scale: Geophysical Methods for Groundwater Evaluation and Management I Posters</b>	

1:40 PM-6:00 PM	<b>NS33A-1582. Geophysical monitoring of ground moisture within a clayey landslide</b> <u>G. Bièvre</u> ; L. Oxarango; D. Jongmans; S. Grangeon; C. Hung; S. Palma-Lopes
1:40 PM-6:00 PM, Halls A-C (Moscone South), <b>T33F. Rock Physical Properties in Fault Zones Through the Seismic Cycle and Implications for Earthquake Dynamics I Posters</b>	
1:40 PM-6:00 PM	<b>T33F-2486. Numerical Investigation of Weak Grains in Granular Shear Zones</b> <u>A.P. Rathbun</u> ; F. Renard; S. Abe
1:40 PM-6:00 PM, Halls A-C (Moscone South), <b>V33A. Constraining the Dynamics of Volcanic Jets and Plumes I Posters</b>	
1:40 PM-6:00 PM	<b>V33A-2619. Jet dynamics at Lone Star Geyser, Yellowstone National Park</b> <u>L. Karlstrom</u> ; M.L. Rudolph; J. Vandemeulebrouck; F. Murphy; S. Hurwitz; M. Manga; R.A. Sohn; M.J. Johnston
1:40 PM-3:40 PM, Room 3011 (Moscone West), <b>C33G. Sea Ice Processes and Properties II</b>	
2:40-2:55 PM	<b>C33G-05. Recent mechanical weakening of the Arctic sea ice cover as revealed from larger inertial oscillations. Observations and Analytical Modelling.</b> <u>F. Gimbert</u> ; N. Jourdain; D. Marsan; J. Weiss; B. Barnier
4:00 PM-5:00 PM, Room 3024 (Moscone West), <b>DI34A. Geomagnetic Variability: Origins, Implications, and Predictions II</b>	
4:15-4:30 PM	<b>DI34A-02. Information on the Motions within the Earth's Core and on the Geomagnetic Field prior to Geomagnetic Data Inversion (<i>Invited</i>)</b> <u>D. Jault</u> ; N. Gillet; N. Schaeffer
4:00 PM-6:00 PM, Room 2016 (Moscone West), <b>T34C. New Constraints on Active Fault Zones II</b>	
4:30-4:45 PM	<b>T34C-03. Finding the buried memory of past earthquakes with geophysical, GPR-based paleoseismology</b> <u>I. Manighetti</u> ; S. Beaupretre; S. Garambois; J. Malavieille; M. Chatton; G. Sénéchal

Thursday, December 08, 2011

Time	Session Info
8:00 AM-12:20 PM, Halls A-C (Moscone South), <b>C41E. Monitoring Changes in Polar Ice Sheets and Sea Ice Using Airborne and Satellite Remote Sensing I Posters</b>	
8:00 AM-12:20 PM	<b>C41E-0476. A New Design for Digital Elevation Models of Bedrock Underlying Ice Sheets</b> <u>A. Drouet</u> ; G. Durand; F. Gillet-chaulet; E. Le Meur; J. Braun; M. Sacchetti; D.A. Young; D.D. Blankenship; J. Greenbaum; A. Wright; E.J. Rignot; Y. Gim; J. Mougnot; D. Kirchner

8:00 AM-12:20 PM, Halls A-C (Moscone South), <b>EP41B. Innovative Isotope Methods for Characterization of Earth Surface Processes I Posters</b>	
8:00 AM-12:20 PM	<b>EP41B-0610. Large Nd-Hf isotopic decoupling in Himalayan River Sediments</b> <u>M. Garcon</u> ; C. Chauvel; C. France-Lanord
8:00 AM-12:20 PM, Halls A-C (Moscone South), <b>GP41A. Crustal Imaging With Potential Fields: Applications to Tectonics, Hazards, and Resources III Posters</b>	
8:00 AM-12:20 PM	<b>GP41A-0980. Signature of hydrothermal alteration in ground-magnetic surveys at Yellowstone National Park</b> C. Bouligand; <u>J.M. Glen</u> ; D.K. McPhee
8:00 AM-12:20 PM, Halls A-C (Moscone South), <b>S41A. 3D Seismic Imaging I Posters</b>	
8:00 AM-12:20 PM	<b>S41A-2160. Lithospheric imaging from teleseismic data by frequency-domain elastic full-waveform tomography</b> <u>D. Pageot</u> ; S. Operto; M. Vallée; R. Brossier; J. Virieux
8:00 AM-12:20 PM, Halls A-C (Moscone South), <b>S41B. Application of Natural Source Seismology in the Search for Natural Resources I Posters</b>	
8:00 AM-12:20 PM	<b>S41B-2192. Seismic Surface-wave Tomography From Cross-correlations Of Ambient Noise At The Valhall Oil Field.</b> <u>A. Mordret</u> ; M. Landès; N.M. Shapiro; S.C. Singh; P. Roux; O.I. Barkved
8:00 AM-12:20 PM, Halls A-C (Moscone South), <b>V41C. Peridotites and Serpentinites From Ridges to Subduction Zones: The Role of Fluids at Low and High Temperatures I Posters</b>	
8:00 AM-12:20 PM	<b>V41C-2503. MINERALOGICAL AND GEOCHEMICAL EVOLUTION OF ALPINE SERPENTINITES DURING SUBDUCTION DYNAMICS</b> <u>S. Schwartz</u> ; R. Lafay; F. Deschamps; S. Guillot; C. Nicollet
8:00-8:00 AM	<b>V41C-2513. Origin of multiple serpentinization events in New Caledonia</b> <u>M. Ulrich</u> ; S. Guillot; M. Muñoz; C. Picard
8:00 AM-12:20 PM, Halls A-C (Moscone South), <b>V41D. Role of Fluids in Subduction Processes I Posters</b>	
8:00 AM-12:20 PM	<b>V41D-2531. Dehydration reactions, mass transfer and rock deformation relationships during subduction of Alpine metabauxites: insights from LIBS compositional profiles between metamorphic veins</b> <u>A. Verlaquet</u> ; F. Brunet; B. Goffe; D. Menut; N. Findling; C. Poinssot
8:00 AM-10:00 AM, Room 2012 (Moscone West), <b>T41B. Localized Volumetric Deformation in the Earth's Crust II</b>	
9:12-9:24 AM	<b>T41B-07. Development of roughness in pressure solution interfaces and consequence for the ductile rheology of the upper crust (<i>Invited</i>)</b> <u>F. Renard</u> ; J. Gratier; D.K. Dysthe
8:00 AM-10:00 AM, Room 3005 (Moscone West), <b>NS41A. Exploiting GPR and Seismic Wavefield Properties for Characterization of the Shallow Subsurface I</b>	

9:30-9:45 AM	<b>NS41A-06. Small scale seismic measurement bench to assess imaging methods – application to Full Waveform Inversion of a shallow structure.</b> D. Leparoux; <u>F. Bretaudeau</u> ; R. Brossier; S. Operto; J. Virieux
10:20 AM-12:20 PM, Room 304 (Moscone South), <b>NG42A. Turbulence in Geophysical and Astrophysical Fluid Dynamics II</b>	
10:50-11:05 AM	<b>NG42A-03. A dynamo driven by zonal jets at the upper surface: applications to giant planets (<i>Invited</i>)</b> <u>C. Guervilly</u> ; P. CARDIN; N. Schaeffer
10:20 AM-12:20 PM, Room 2016 (Moscone West), <b>T42C. Rock Physical Properties in Fault Zones Through the Seismic Cycle and Implications for Earthquake Dynamics II</b>	
11:20-11:35 AM	<b>T42C-05. Rheological Evolution of Faults During the Seismic Cycle: the Role of Pressure Solution Creep and Sealing Processes</b> <u>J. Gratier</u> ; F. Renard; J. Richard; M. Doan; B. Vial
1:40 PM-6:00 PM, Halls A-C (Moscone South), <b>S43B. Research and Development in Nuclear Explosion Monitoring II Posters</b>	
1:40 PM-6:00 PM	<b>S43B-2229. Determination of the source time function of seismic event by blind deconvolution of regional coda wavefield: application to December 22, 2009 explosion at Kambarata, Kyrgyzstan</b> <u>O.G. Sebe</u> ; J. Guilbert; P. Bard
1:40-1:40 PM	<b>S43B-2235. Using teleseismic data to improve the depth estimation of the 07th of July 2011 Corsica event</b> <u>J. Letort</u> ; J. Guilbert; J. Vergoz; Y. Cano; O.G. Sebe; F. Cotton
1:40 PM-3:40 PM, Room 307 (Moscone South), <b>V43E. Origin and Evolution of Earth's Crust II</b>	
3:25-3:40 PM	<b>V43E-08. The Lesser Antilles: a case study for melt-dehydration processes in arcs</b> <u>C. Chauvel</u> ; S. Labanieh; M. Carpentier
4:00 PM-6:00 PM, Room 307 (Moscone South), <b>V44B. Origin and Evolution of Earth's Crust III</b>	
5:15-5:30 PM	<b>V44B-06. Scientific Drilling in the Barberton Greenstone Belt, South Africa</b> <u>N. Arndt</u>

Friday, December 09, 2011

Time	Session Info
8:00 AM-12:20 PM, Halls A-C (Moscone South),	<b>H51G. Multiscale and Coupled Complexity in Geologic Carbon Sequestration I Posters</b>

8:00 AM-12:20 PM	<b>H51G-1262. From Nm-Scale Measurements Of Mineral Dissolution Rate To Overall Dissolution Rate Laws: A Case Study Based On Diopside</b> <u>D. Daval</u> ; G. Saldi; R. Hellmann; K. Knauss
8:00 AM-12:20 PM, Halls A-C (Moscone South), <b>NG51D. Statistical Geomechanics of Episodic Events II Posters</b>	
8:00 AM-12:20 PM	<b>NG51D-1673. Damage dynamics inferred from acoustic emissions in a partially frozen rock-wall</b> <u>L. Girard</u> ; S. Gruber; D. Amitrano
8:00 AM-12:20 PM, Halls A-C (Moscone South), <b>NS51B. Near Surface Geophysics General Contributions III Posters</b>	
8:00 AM-12:20 PM	<b>NS51B-1746. Modeling and inversion Matlab algorithms for resistivity, induced polarization and seismic data.</b> <u>M. Karaoulis</u> ; A. Revil; B.J. Minsley; D.D. Werkema
8:00 AM-12:20 PM, Halls A-C (Moscone South), <b>DI51B. Terrestrial Planetary Cores II Posters</b>	
8:00 AM-12:20 PM	<b>DI51B-2139. Seismic anisotropy of the inner core deduced from geodynamical and mineralogical models</b> <u>P. CARDIN</u> ; A. Lincot; S. Merkel; R. Deguen
8:00 AM-12:20 PM, Halls A-C (Moscone South), <b>MR51A. Mineral and Rock Physics General Contributions Posters</b>	
8:00 AM-12:20 PM	<b>MR51A-2159. Uncertainty of permeability and specific storage due to experimental error during data acquisition for pulse-transient technique</b> <u>I. Song</u> ; A.P. Rathbun; D.M. Saffer
8:00 AM-10:00 AM, Room 2018 (Moscone West), <b>V51I. Peridotites and Serpentinites From Ridges to Subduction Zones: The Role of Fluids at Low and High Temperatures II</b>	
8:30-8:45 AM	<b>V51I-03. MASS TRANSFERS DURING SERPENTINIZATION OF OCEANIC PERIDOTITES (<i>Invited</i>)</b> <u>M. Andreani</u> ; M. Godard; A. Delacour; J. Escartin; C. Mevel; M. Muñoz
8:00 AM-10:00 AM, Room 2007 (Moscone West), <b>V51G. Cyclic Activity and Flow Instability in Volcanoes, Geysers, and Mud Volcanoes I</b>	
9:15-9:30 AM	<b>V51G-06. On the relationship between Very-Long-Period events, bubble collapse, and eruption processes at the Lone Star Geyser, Yellowstone National Park</b> <u>R.A. Sohn</u> ; J. Vandemeulebrouck; S. Hurwitz; M.J. Johnston; L. Karlstrom; M.L. Rudolph; F. Murphy; C. Pontbriand; G. Horning
9:30-9:45 AM	<b>V51G-07. Interpretation of seismic signals at Lone Star Geyser in the context of surface activity using visible and infrared video (<i>Invited</i>)</b> <u>M.L. Rudolph</u> ; J. Vandemeulebrouck; S. Hurwitz; L. Karlstrom; M.J. Johnston; M. Manga; R.A. Sohn

9:45-10:00 AM	<b>V51G-08. Self-potential, Ground-tilt and Infra-Red Emission Associated with Geyser Eruptions: Implications for Volcanic Monitoring.</b> <u>M.J. Johnston</u> ; S. Hurwitz; R.A. Sohn; J. Vandemeulebrouck; L. Karlstrom; M.L. Rudolph
10:20 AM-12:20 PM, Room 2007 (Moscone West), <b>V52B. Geophysical Observations of Stress-Strain Changes at Active Volcanoes I</b>	
10:20-10:35 AM	<b>V52B-01. Forward and Inverse Modeling of the seismic and electromagnetic disturbances associated with localized seismic sources in volcanic areas (Invited)</b> <u>A. Revil</u> ; H. Mahardika; A. Jardani
10:50-11:05 AM	<b>V52B-03. Magma replenishment and volcanic unrest inferred from the analysis of VT micro-seismicity and seismic velocity changes at Piton de la Fournaise Volcano</b> <u>F. Brenguier</u> ; E. Rivemale; D.S. Clarke; A. Schmid; J. Got; J. Battaglia; B. Taisne; T. Staudacher; A. Peltier; N.M. Shapiro; S. Tait; V. Ferrazzini; A. Di Muro
1:40 PM-6:00 PM, Halls A-C (Moscone South), <b>V53A. Cyclic Activity and Flow Instability in Volcanoes, Geysers, and Mud Volcanoes II Posters</b>	
1:40 PM-6:00 PM	<b>V53A-2582. Periodic flow instabilities during Lone Star Geyser (YNP) eruptions, as deduced from acoustic measurements.</b> <u>J. Vandemeulebrouck</u> ; S. Hurwitz; M.J. Johnston; M.L. Rudolph; L. Karlstrom; R.A. Sohn; F. Murphy; D.K. McPhee; J.M. Glen; S.A. Soule; C.M. Meertens
1:40-1:40 PM	<b>V53A-2583. Direct Measurement of the Volume of Liquid Water Emitted During Eruptions of Lone Star Geyser, Yellowstone National Park, Wyoming</b> <u>F. Murphy</u> ; S. Hurwitz; M.J. Johnston; J. Vandemeulebrouck; C. Pontbriand; R.A. Sohn; L. Karlstrom; M.L. Rudolph
1:40-1:40 PM	<b>V53A-2584. A Multi-Method Experiment to Investigate Geyser Dynamics: Lone Star Geyser, Yellowstone National Park</b> <u>S. Hurwitz</u> ; J. Vandemeulebrouck; M.J. Johnston; R.A. Sohn; L. Karlstrom; M.L. Rudolph; F. Murphy; D.K. McPhee; J.M. Glen; S.A. Soule; C. Pontbriand; C.M. Meertens
1:40 PM-6:00 PM, Halls A-C (Moscone South), <b>V53C. Geophysical Observations of Stress-Strain Changes at Active Volcanoes II Posters</b>	
1:40 PM-6:00 PM	<b>V53C-2635. Volcano-tectonic earthquake source mechanisms during magma ascent at Piton de la Fournaise volcano.</b> <u>A. Schmid</u> ; P. Lemarchand; F. Brenguier; O. Coutant; A. Maggi
1:40 PM-6:00 PM, Halls A-C (Moscone South), <b>V53E. Surveillance of Volcanic Unrest: New Developments in Multidisciplinary Monitoring Methods IV Posters</b>	

1:40 PM-6:00 PM	<b>V53E-2665. Muon tomography of the Soufrière of Guadeloupe (Lesser Antilles): Comparison with other geophysical imaging methods and assessment of volcanic risks.</b> D. Gibert; N. Lesparre; J. Marteau; <u>B. Taisne</u> ; F. Nicollin; O. Coutant
1:40 PM-3:40 PM, Room 104 (Moscone South), <b>U53E. Climate Loads as Forcers of Seismic and Volcanic Processes II (Video On-Demand)</b>	
2:20-2:40 PM	<b>U53E-03. Climate effects on volcanism: Influence of ice load variations on magma storage zones with application to Icelandic volcanoes. (Invited)</b> <u>F. Albino</u> ; V. Pinel; F. Sigmundsson
4:00 PM-6:00 PM, Room 304 (Moscone South), <b>GP54A. Magnetostratigraphy and Remagnetization of Sediments III</b>	
5:12-5:24 PM	<b>GP54A-06. Pyrrhotite remagnetizations in Himalayan rocks</b> <u>E. Appel</u> ; C. Crouzet; E. Schill

Final ID: T11D-01

**Coupling Climate, Surface Processes and Mantle Convection (*Invited*)**

*R. Moucha*<sup>1</sup>; *J. Braun*<sup>2</sup>; *A. M. Forte*<sup>3</sup>; *A. B. Bush*<sup>4</sup>; *D. B. Rowley*<sup>5</sup>; *F. Guillocheau*<sup>6</sup>; *C. Robin*<sup>6</sup>;

1. Department of Earth Sciences, Syracuse University, Syracuse, NY, United States.
2. ISTerre, Université Joseph Fourier de Grenoble et Institut Universitaire de France, Grenoble, France.
3. GEOTOP, Université du Québec à Montréal, Montréal, QC, Canada.
4. Department of Earth and Atmospheric Sciences, University of Alberta, Edmonton, AB, Canada.
5. Department of the Geophysical Sciences, University of Chicago, Chicago, IL, United States.
6. Géosciences Rennes, Université de Rennes 1, Rennes , France.

**Body:** The geological record contained in sedimentary basins and continental margins can provide a strong constraint on the Earth's surface geological and climatic evolution, as well as offer an indication of deep Earth dynamics. However, the long-term tectonic signal present in the sedimentary record is a convolution of the complex interactions of the mantle, the crust and surface processes, where the latter are controlled by the dynamics of the atmosphere and sea level change. Therefore, to unravel this record, a multidisciplinary approach is essential. Herein we combine models of the past climate constrained by geology with a large-scale surface processes model for erosion and sediment transport (TopoSed; Simoes et al., 2010) in which the long-term tectonic uplift and subsidence is retrodicted by a global mantle convection model (Moucha et al., 2011). We focus on the topographic evolution of the late Cenozoic African continent and quantify the relative contributions of climate, rock erodibility, mantle rheology, and present-day mantle heterogeneity in terms of the modeled sediment supply to the margins and compare this with the observed sedimentary fluxes inferred from the geological record.

Final ID: U13A-0029

## Geochemical and petrological study of Barberton Greenstone Belt cherts (3.2-3.5 Ga), South Africa

*M. Ledevin*<sup>1</sup>; *N. Arndt*<sup>1</sup>; *A. Simionovici*<sup>1</sup>;

1. ISTERre, Grenoble Cedex 9, France.

**Body:** The massive deposition of cherts during Archean time provides important information about conditions on the sea floor during the early history of the Earth. We studied samples from four sites in the Barberton Greenstone Belt (3.2-3.5 Ga), South Africa, including fresh ICDP core samples, to understand their formation. We identified three different origins for cherts: direct precipitation from seawater, precipitation in fractures from silica-rich fluids, and replacement of preexisting rocks (silicification) at or near the surface.

To better constrain the various formation processes of cherts, we use a petrological, rheological and geochemical approach: both macro- and micro- structural observations are used to understand early physical behavior of chert, silica precipitation, and silicification processes. Rheological information is obtained by careful field observations: we observe a complex behavior for cherts, with ductile to brittle deformation structures, sometimes both in the same layer, extremely fast diagenetic induration processes, and evidence of an early colloidal silica phase. High-resolution analyses (RAMAN, synchrotron and lab-based X-Ray microfluorescence, cathodoluminescence) are used to link micro-scale element distribution with microstructures, and to understand micro-scale formation processes. These approaches will be complemented by stable isotope (Si and O) and fluid inclusions analyses.

Coupling petrological informations and geochemical analyses allow us to define reliable criteria to differentiate the three origins of cherts. When petrological observations show a secondary silicification of previously deposited sediments (e.g. laminations, ripple marks, silicified ashes), samples have trace element patterns with high HREE contents, and strong negative Sr and Li anomalies. In comparison, when cherts seem to be chemically precipitated on the sea floor, patterns show lower HREE and higher LILE contents, with a strong positive Ba anomaly and depletion in Zr and Hf. Some commonly used criteria to identify the origin of fluids, such as Eu positive anomaly as a hydrothermal signal and Y, La and Gd positive anomalies and enrichment in HREE contents as oceanic signals, appear unreliable.

We also undertook a petrological and geochemical study of siliceous chemical precipitates in modern volcanic lakes. Comparison of internal structures and chemical signatures of Archean and modern cherts is used to constrain rheological properties, to infer early physico-chemical conditions on the seafloor, and to study fractionation processes during silica transfer from fluid to rock.

Final ID: H13A-1188

## Reservoir-Seal-Fault Systems Leakage Evolution Through Time and Space

*E. Frery*<sup>1,2</sup>; *N. Ellouz*<sup>1</sup>; *J. Gratier*<sup>2</sup>; *P. Deschamps*<sup>3</sup>;

1. IFP energies nouvelles, Rueil Malmaison, France.

2. LGIT, Grenoble, France.

3. CEREGE, Aix-en-Provence, France.

**Body:** Thanks to the study of natural CO<sub>2</sub> reservoirs, tools are developed in order to understand the CO<sub>2</sub> storage efficiency and long-term evolution.

The Colorado Plateau red sandstones, in southern Utah, are marked by fluid driven mineralization and alteration along joints, fractures and faults. These traces are considered as evidences for paleo and present-day migration pathways of the exotic fluids coming from reservoirs (located at different depths) to the surface across or along the transfer faulted zones. Understanding these mechanisms through time is crucial not only in the determination of the fault activity, for identifying the transient and permanent processes along this fault system, but also in the long-term paleo-sequestration calibration, and finally in the evaluation of hydrocarbon, gas, water and CO<sub>2</sub> migration.

In order to investigate the nature and the origin of the different leaking fluids or gas, we conducted a study along Moab and Green River Fault systems, from Moab to the western side of the San Raphael Swell, in Utah.

A geological fieldwork highlights several former and current transfer and leakage processes, evidenced by (1) chemical bleaching, (2) gypsum, (3) different kinds of oxides, (4) carbonate precipitations, and (5) present day CO<sub>2</sub> expulsion located all along the faults traces from Jurassic units to the present-day surface. Due to the different erosion pattern in the area, access to several reservoir and seals was possible for observation and sampling. This first step allowed to characterize the orientation and position of each leaky fluid family, and to analyze the fluids and carbonate precipitation with respect to the structural context. For instance, the strong impact of salt tectonics implies that some of the faults are probably rooted within this decollement, and that a system of small wavelength syncline/anticline is added a significant variability to the drainage pattern of these faults.

In order to define the nature and the origin of the fluids responsible for the traces and seepages observed, we used a multi-disciplinary approach using the different following methods coming from: geology, geochemistry, petrography, XRD, trace elements analyses and U/Th datings.

Finally, so as to understand the link between flow and tectonic histories of the reservoir-seal-fault systems, we integrate the analytical and the structural data set. This last step allows to propose a precise chronology and history of the fluid leakage in this western part of the Colorado Plateau, from Jurassic to present day. These combined technical methodologies represents a great tool to understand the leaking, and remediation processes, to characterize the variation through time and space of the fault activity and finally to evaluate the lost volume from reservoirs along a major fault system.

**Origin of fault roughness and the development of slip surfaces**

T. Candela<sup>1</sup>; F. Renard<sup>2, 3</sup>;

1. Department of Earth and Planetary Sciences, University of California–Santa Cruz, Santa Cruz, CA, United States.

2. ISTerre, University Joseph Fourier – Grenoble I & CNRS, Grenoble, France.

3. Physics of Geological Processes, University of Oslo, Oslo, Norway.

**Body:** The compiled results of our analysis and previous works indicate that the roughness of active fault scarps follows a single self-affine regime with no characteristic length scale from the micrometer scale to 30 m, independently of the geological setting. More precisely, the fault surface topography along the slip direction can be characterized by a universal Hurst exponent:  $H_{para} = 0.6$ . This means that the standard deviation of the roughness amplitude scale as  $L^{0.6}$  where  $L$  is the distance along the fault. Here, we interpret this observation by the fact that faulting roughness generation is dominated by elastic (i.e. brittle) processes for which no intrinsic scale exists and that these elastic processes can leave an imprint on the fault geometry in the form of elongated lenses that we have characterized. Fault zones studied show a similar structure damage, characterized by an anastomosed network of multi-scale sliding surfaces individualizing lenses of damaged rock. It appears that fault surfaces, for which we have characterized the roughness, are in fact constituted of many discrete slip surfaces delimiting bumpy lenses elongated in the direction of slip. Symmetry axes measurements of the lenses of the Dixie Fault (Nevada) reveals that their geometry is scale dependent. Indeed, the thickness  $T$  of the lenses scales with their length  $l$  (measured in the slip direction) as  $T \propto l^{0.6}$ . Based on experimental works on the fault growth which observed similar results, we propose that the multi-scale aggregation of lenses explains the observation that the standard deviation of the roughness amplitude of the fault surface scales as  $L^{0.6}$ . It appears that elastic interactions related to branching of many discrete slip surfaces, controlling the generation of the multi-scale bumpy lenses, could be the scale-free process at the origin of fault roughness. In addition, the elastic interactions should be relatively greater at smaller scales in order to explain that the geometry of the lenses (resulting from the branching of the multi-scale slip surfaces) scales as  $T \propto l^{0.6}$ , and that their multi-scale aggregation is at the origin of the self-affine regime of fault roughness.

Final ID: G14A-07

**Interseismic coupling and block motion along the northern Peru and southern Ecuador subduction zone (*Invited*)**

*F. Rolandone*<sup>1</sup>; *J. Nocquet*<sup>2</sup>; *J. Villegas Lanza*<sup>2, 3</sup>; *P. A. Mothes*<sup>4</sup>; *D. Cisneros Revelo*<sup>5</sup>; *M. Chlieh*<sup>2</sup>; *L. Audin*<sup>6</sup>; *H. Tavera*<sup>3</sup>; *P. Jarrin*<sup>4</sup>; *E. O. Norabuena*<sup>3</sup>; *F. Bondoux*<sup>7</sup>;

1. ISTEP , Univ Pierre et Marie Curie, Paris, France.
2. GeoAzur, Univ. Nice-CNRS-IRD-OCA , Valbonne, France.
3. Instituto Geofísico del Peru, Lima, Peru.
4. Instituto Geofísico, Escuela Politécnica Nacional, Quito, Ecuador.
5. Instituto Geografico Militar, Quito, Ecuador.
6. IRD-ISterre, Grenoble, France.
7. IRD-GET, Toulouse, France.

**Body:** We use GPS measurements in the first geodetic study of the Nazca/South America subduction zone along northern Peru and southern Ecuador (from 1°S to 10°S). Rapid subduction of the Nazca plate (~ 6 cm/yr) under the northern Andes margin gives rise to heterogeneous interseismic plate interface coupling, changing with latitude. Very weak to null coupling is found along a 800 km long segment (from 1°S to 9°S) indicating that this segment is slipping mostly aseismically. South of 9°S, a strong coupling is observed, indicating a nearly fully locked subduction zone. These two segments are characterized by a change in the seismicity. Large to great earthquakes occur south of 10°S. Their ruptures zones do not extend further north and do not cross the Mendana fracture zone, which may act as a barrier. The Mendana fracture zone also correlates with the change from high to weak coupling determined from GPS. On the contrary no large earthquakes are documented in the weakly coupled northern segment. However, two unusual shallow tsunami earthquakes, with long rupture durations and shallow depths, occurred in 1960 (Mw 7.6) and 1996 (Mw 7.5), and are consistent with the hypothesis of very shallow coupling along the trench. Finally, the GPS velocity field shows a surprising result, that is a ~5 mm/yr consistent southeastwards motion of a continental block with little internal deformation, extending further north in Ecuador. The existence of this block had not been anticipated in previous studies and leads us to reassess the seismic potential of continental faults in the overriding plate.

Final ID: S21D-04

INVESTIGATING TRIGGERING IN SEISMICITY PATTERNS; THE SPECIAL CASE OF TRIGGERING DISTANCE DISTRIBUTIONS (*Invited*)

D. Marsan<sup>1</sup>;

1. Université de Savoie, ISTerre, Le Bourget du Lac, France.

**Body:** Earthquake interactions are responsible for seismicity patterns, but analyzing patterns to understand interaction processes is unfortunately not straightforward. Small earthquakes contribute significantly to the triggering of subsequent earthquakes, making the identification of the causative trigger a particularly difficult task. We will here describe recent methods that aim at practically deciphering the causal triggering links between earthquakes. We will then apply these methods to determine the distribution of distance between the triggering and the triggered earthquake. A power-law can describe this distribution, with an exponent that do not significantly change with the time between the two events. We suggest that, according to the rate-and-state friction model, static stress triggering can explain this distribution.

Final ID: S22B-07

**Link between Coulomb stress changes and seismic activation in the Marmara sea after the Izmit (Turkey) earthquake**

*V. Durand*<sup>1</sup>; *M. P. Bouchon*<sup>1</sup>; *H. Karabulut*<sup>2</sup>; *J. Schmittbuhl*<sup>3</sup>; *D. Marsan*<sup>4</sup>;

1. ISTERRE, Université de Grenoble, Centre National de la Recherche Scientifique, Grenoble, France.
2. Kandilli Observatory and Earthquake Research Institute, Istanbul, Turkey.
3. IPGS, Université de Strasbourg, Centre National de la Recherche Scientifique, Strasbourg, France.
4. ISTERRE, Université de Savoie, Le Bourget-du-Lac, France.

**Body:** We have investigated the role of the dynamic and static stress changes after the 1999 Izmit earthquake, on four pre-existing seismic clusters located in the eastern Marmara sea, beyond the western end of the earthquake rupture. These four clusters show long-lasting modifications in their seismicity rate. We observe that these seismic activity variations are strongly related to the stress changes. Where the dynamic stress changes are important, the activation is instantaneous, whereas when the static stress changes are positive and large, the activation lasts longer. When static stress changes are negative, we observe the appearance of a seismicity shadow. However, one of the clusters, the Yalova cluster, does not reply in this way. In spite of a negative stress change, its activity is strongly increased for a long duration. We infer that this activation is due to an increase of the pressure after the earthquake. We also highlight that the delay of activation is linked to the type of faulting. Clusters located on the strike-slip faults are immediately activated, whereas the extensional ones are activated after a delay.

Final ID: G23A-0841

**The 2009-2010 Guerrero Slow Slip Event Monitored by InSAR, Using Time Series Approach.**

*G. Bacques*<sup>1, 2</sup>; *E. Pathier*<sup>1</sup>; *C. Lasserre*<sup>1</sup>; *F. Cotton*<sup>1</sup>; *M. Radiguet*<sup>1</sup>;

1. ISTERre, Grenoble, 38000, France.

2. CNES, Paris, 75000, France.

**Body:** The Guerrero seismic gap is located along the Pacific coast of Mexico in a subduction zone where Cocos plate subducts under the North American plate with a 5.5 cm per year convergence rate. Along this 100 km width band located between Acapulco (East side) and Zihuatanejo (West side), no major earthquake occurred since at least 1911. In contrast, the surrounding areas of the Guerrero gap has been the location of large seismic events during the last century like the 1985 one's (Mw 8), which affected Mexico City. Considering the plate convergence rate, a 5 meters slip deficit has been estimated at this gap location since the last major earthquake (Lowry et al. 1998), making a large earthquake possible at this spot. However, the Guerrero gap was the setting of four slow slip events (SSE) with an approximately four years periodicity (1998, 2002, 2006, 2009-2010) since it was instrumented by GPS permanent network in January 1997. Slow slip events and their associated ground displacements are commonly interpreted as aseismic slips on the deeper part of the subduction plane. One of the main issues concerning that phenomenon, deals with the way that strain accumulated on the deeper part is released on the upper part of the subduction plane, which corresponds to the seismogenic zone. As a consequence, the slip distribution upon the subduction plane associated to the Guerrero SSE represents relevant information concerning the local seismic hazard. To address this issue, geodetic measurements from GPS and/or space-borne SAR differential interferometry (DInSAR) can be used to retrieve the SSE slip distribution on the subduction plane from the ground deformation measurements as it has been done for the 2006 event previously studied. In this work, we focused on the 2009-2010 SSE on Guerrero by processing DInSAR data (C band Envisat data were processed using the small baseline approach method NSBAS based upon ROI-pac) as previously done for the 2006 event but improved by adding a Time Series approach. Time Series approach is useful for monitoring ground deformation evolution during the slow slip events and makes the slip propagation mapping upon the subduction plane a promising goal. Here we present our first results concerning the 2009-2010 slow slip events, particularly the distribution of the cumulative surface displacement in LOS (satellite Line Of Sight), the slip distribution associated on the fault plane and the ground deformation evolution obtained. Finally, we open the discussion with a first comparison between the 2009-2010 and the 2006 events that reveal some differences concerning the amplitude and the distribution of the ground deformation.

**Comparison between two methods for forward calculation of ambient noise H/V spectral ratios**

*A. Garcia-Jerez*<sup>1</sup>; *F. Luzón*<sup>1</sup>; *F. J. Sanchez-Sesma*<sup>2</sup>; *M. A. Santoyo*<sup>3</sup>; *D. Albarello*<sup>4</sup>; *E. Lunedei*<sup>4</sup>; *M. Campillo*<sup>5</sup>; *U. Iturrarán-Viveros*<sup>2</sup>;

1. Univ. de Almeria, Almeria, Spain.
2. UNAM, DF, Mexico.
3. UCM, Madrid, Spain.
4. Univ. di Siena, Siena, Italy.
5. Univ. Joseph Fourier, Grenoble, France.

**Body:** The analysis of horizontal-to-vertical spectral ratios of ambient noise (NHVSR) is a valuable tool for seismic prospecting, particularly if both a dense spatial sampling and a low-cost procedure are required. Unfortunately, the computation method still lacks of a unanimously accepted theoretical basis and different approaches are currently being used for inversion of the ground structure from the measured H/V curves.

Two major approaches for forward calculation of NHVSRs in a layered medium are compared in this work. The first one was developed by Arai and Tokimatsu (2004) and recently improved by Albarello and Lunedei (2011). It consists of a description of the wavefield as generated by Far Surface point Forces (FSF method). The second one is based on the work of Sánchez-Sesma et al. (2011) who consider ambient noise as a Diffuse WaveField (DWF method), taking advantage of the proportionality between its Fourier-transformed autocorrelation (power spectrum) and the imaginary part of the Green function when source and receiver are the same.

In both methods, the NHVSR is written as  $(P_H/P_V)^{1/2}$ , where  $P_H$  and  $P_V$  are the horizontal and vertical power spectra. In the FSF method these quantities are given by

$$P_V \propto \sum_m (1 + \frac{1}{2} \chi_m^2 \alpha^2) (A_{Rm}/k_{Rm})^2$$
$$P_H \propto \sum_m \{ (1 + \frac{1}{2} \chi_m^2 \alpha^2) (A_{Rm}/k_{Rm})^2 \chi_m^2 + \frac{1}{2} \alpha^2 (A_{Lm}/k_{Lm})^2 \}$$

where  $k_{Rm}$ ,  $\chi_m$  and  $A_{Rm}$  are wavenumber, ellipticity and medium response of the m-th Rayleigh wave mode;  $k_{Lm}$  and  $A_{Lm}$  correspond to the m-th Love wave mode and  $\alpha$  is the horizontal-to-vertical load ratio of the ambient noise sources. Some common factors are omitted in the expressions of  $P_V$  and  $P_H$ .

On the other hand, the DWF method deals with the full wavefield including both surface and body waves. In order to make the comparison easier, and taking into account that surface waves are often the dominant components in wide spectral ranges, body wave contributions are neglected here. In this case, the  $P_H$  and  $P_V$  power spectra for the DWF method are reduced to the simple expressions:

$$P_V = \frac{1}{2} \sum_m A_{Rm}$$
$$P_H = \frac{1}{2} \sum_m (A_{Rm} \chi_m^2 + A_{Lm})$$

Thus, the main difference between these methods is the way in which the amount of energy injected in each surface

wave mode is established: either following the energy equipartition principle (DWF method) or controlled by surface point loads with angle  $\tan^{-1} \alpha$  (FSF method).

These methods have been numerically compared for a simple structure consisting of a plane layer overlaying a halfspace. S-wave velocity contrast was varied between 2 and 6, and Poisson ratios of the layer from 0.25 to 0.45 (using 0.25 for the halfspace). We set  $\alpha=1$  for the FSF method. Although both methods provide NHVSRs of similar shape and very close peak frequencies, peaks obtained from DWF are significantly smoother. Both ratios become constant as frequency increases, but their high frequency limits differ too.

## References

Albarello, D. & E. Lunedei (2011). Near Surface Geophysics 9, In press.

Arai, H. & K. Tokimatsu (2004). Bull. Seismol. Soc. Am. 94, 53–63.

Sánchez-Sesma, F. J., M. Rodríguez, U. Iturrarán-Viveros, F. Luzón, M. Campillo, L. Margerin, A. García-Jerez, M. Suarez, M. A. Santoyo & A. Rodríguez-Castellanos (2011). Geophys. J. Int. 186, 221–225.

Final ID: S23B-2263

**Temporal variations of non-volcanic tremor (NVT) locations in the Mexican subduction zone: finding the NVT sweet spot**

*A. L. Husker*<sup>1</sup>; *V. Kostoglodov*<sup>1</sup>; *V. M. Cruz-Atienza*<sup>1</sup>; *D. Legrand*<sup>1</sup>; *N. M. Shapiro*<sup>2</sup>; *J. S. Payero*<sup>1</sup>; *M. Campillo*<sup>3</sup>; *E. Huesca-Perez*<sup>1</sup>;

1. Instituto de Geofísica, U.N.A.M., Mexico City, DF, Mexico.

2. IPGP, Paris, France.

3. CNRS, Univ Joseph Fourier, Grenoble, France.

**Body:** Epicentral locations of non-volcanic tremors (NVT) in the Mexican subduction zone are determined from the peak of the measured energy and examined over time. From this data NVT is found to occur continuously at a distance of ~215 km from the trench, which we term the “Sweet Spot” because this region probably has the most plausible conditions (proper pressure, fluid content, temperature ~500 °C at the plate interface, and shear stress) for the NVT to always occur. High energy NVT bursts are also observed every few months, extending ~180 km to ~220 km from the trench with durations of a few weeks. During the 2006 slow slip event the duration and frequency of the NVT bursts increased and low energy bursts were observed ~150 km to ~180 km from the trench. We suggest that small, short term slow slip events (SsE) generate additional shear stress creating the high energy NVT bursts and allow NVT to occur outside of the Sweet Spot. SsE’s were triggered by the large, long term 2006 slow slip event (SSE) as evidenced by the increase in frequency and duration of the high energy NVT.

Final ID: S23B-2264

### Toward a Unified Theory of Silent Seismicity in Central Mexico

*V. M. Cruz-Atienza*<sup>1</sup>; *D. N. Rivet*<sup>2</sup>; *V. Kostoglodov*<sup>1</sup>; *A. L. Husker*<sup>1</sup>; *D. Legrand*<sup>1</sup>; *M. Campillo*<sup>2</sup>;

1. Sismología, Instituto de Geofísica, UNAM, Mexico DF, Mexico.

2. Institut des Sciences de la Terre (ISTerre), Grenoble, France.

**Body:** During the 2006 slow slip event (SSE) in Guerrero, Mexico, a seismic profile was deployed above the slipping interface. Data from this seismological network generated several observations, including the detection of an ultra-slow velocity layer confined to the uppermost part of the slab (Song et al., *Science*, 2009), high Poisson's and  $V_p/V_s$  ratios within a large slab segment (Kim et al., *JGR*, 2010), and a transient reduction of surface waves velocity in the middle crust of about 0.2% due to the quasi-static slow-slip process (Rivet et al., *GRL*, 2011). Based on these observations, we have proceeded as follow.

The slip history of the 2006 Guerrero SSE (Radiguet et al., *GJI*, 2010) was put into a 3D viscoelastic finite difference code, approximating the pore pressure as  $P_p = B \cdot P_c$ , where  $B$  is the Skempton coefficient ( $0 \leq B \leq 1$ ) and  $P_c$  is the confining pressure. Solving the fluid diffusion equation in the model, we find that the silent earthquake induces a widespread decrease of effective pressure,  $P_e = P_c - P_p$  (i.e. dilation increase), above the horizontal segment of the plate interface, where the NVT activity has been localized by previous authors (Payero et al., *GRL*, 2008; Husker et al., submitted, 2011). Assuming a fluid seal along the plate interface as suggested in Cascadia (Audet et al., *Nature*, 2009), the time-dependent migration (velocity) of confined fluids in the ultra-slow layer is first upward everywhere and then reorganizes by pointing two 'attraction' poles (i.e. low-pressure slab segments), the first one 80-90 km and the second one around 150 km away from the coast.

We present NVT relocations obtained with a new and promising technique (Cruz-Atienza et al., in preparation, 2011). This technique is based on NVT energy-like and waveform correlation measurements in the three ground motion components. By superimposing the hypocentral relocations over the evolving  $P_p$  lithospheric cross-section, a surprisingly good correlation appears between the slab 'attraction' poles and a north-south NVT spatial segmentation, also reported in previous location catalogs. Both the secular and triggered NVT activity during the SSE are localized over widespread regions of the middle crust (~20 km depth), clearly above the plate interface (~40 km depth). The fluid 'attraction' poles are generated by stress concentrations associated with the SSE northernmost slip edge and the kink of the slipping interface where the slab becomes horizontal. Both stress concentrations induce important strain gradients along the slab top layer, which may open hydraulic windows allowing fluids to rise into the overriding plate. The transient velocity change observed during the 2006 SSE (Rivet et al., *GRL*, 2011) is a strong evidence of non-linear processes occurring in the middle crust, which imply a transient reduction of the bulk shear modulus (i.e. material strength) (Johnson and Jia, *Nature*, 2005). Such behavior, which is enhanced for low effective pressures ( $P_e$ ) (i.e. where fluids are present), promotes shear failure and starts happening from deformation thresholds of about 10-6 that we show were clearly overcome during the 2006 SSE in the NVT locus above the plate interface.

Final ID: S23B-2279

**Tectonic Tremor analysis with the Taiwan Chelungpu-Fault Drilling Program (TCDP) downhole seismometer array**

*Y. Lin*<sup>1</sup>; *G. Hillers*<sup>2</sup>; *K. Ma*<sup>1</sup>; *M. Campillo*<sup>2</sup>;

1. Institute of Geophysics, National Central University, Chungli, Taiwan.

2. Institut des Sciences de la Terre, Université Joseph Fourier, Grenoble, France.

**Body:** We study tectonic tremor activity in the Taichung area, Taiwan, analyzing continuous seismic records from 6 short-period sensors of the TCDP borehole array situated around 1 km depth. The low background noise level facilitates the detection of low-amplitude tectonic tremor and low-frequency earthquake (LFE) waveforms. We apply a hierarchical analysis to first detect transient amplitude increases, and to subsequently verify its tectonic origin, i.e. to associate it with tremor signals. The frequency content of tremor usually exceeds the background noise around 2-8 Hz; hence, in the first step, we use BHS1, BHS4 and BHS7 (top, center, bottom sensor) records to detect amplitude anomalies in this frequency range. We calculate the smoothed spectra of 30 second non-overlapping windows taken daily from 5 night time hours to avoid increased day time amplitudes associated with cultural activities. Amplitude detection is then performed on frequency dependent median values of 5 minute advancing, 10 minute long time windows, yielding a series of threshold dependent increased-energy spectra-envelopes, indicating teleseismic waveforms, potential tremor records, or other transients related to anthropogenic or natural sources. To verify the transients' tectonic origin, potential tremor waveforms detected by the amplitude method are manually picked in the time domain. We apply the Brown et al. (2008) LFE matched filter technique to three-component data from the 6 available sensors. Initial few-second templates are taken from the analyst-picked, minute-long segments, and correlated component-wise with 24-h data. Significantly increased similarity between templates and matched waveform segments is detected using the array-average 7-fold MAD measure. Harvested waveforms associated with this initial 'weak' detection are stacked, and the thus created master templates are used in an iterative correlation procedure to arrive at robust LFE detections. The increased similarity of waveforms, showing essentially no moveout across the array, suggests a common source and path effect, therefore increasing the likelihood of a tectonic origin. Preliminary results from a pilot analysis confirm the existence of tremor-like signals in the tremor-typical frequency range. We present results from a comprehensive analysis of at least 2 years of continuous data. A limited resolution location procedure is applied, testament to the receiver geometry, and the inferred locations are discussed in relation to the tectonic situation.

Final ID: T23C-2412

### **Spatial and temporal evolution of aseismic slip along the Haiyuan fault from SAR interferometry**

*R. Jolivet*<sup>1</sup>; *C. Lasserre*<sup>1</sup>; *T. Candela*<sup>1</sup>; *F. Renard*<sup>1, 2</sup>; *M. Doin*<sup>3</sup>; *G. Peltzer*<sup>4</sup>;

1. ISTerre, Université Joseph Fourier, Grenoble, 38041, France.

2. Physics of Geological Processes, University of Oslo, Oslo, Norway.

3. Laboratoire de Géologie, Ecole Normale Supérieure, Paris, 75005, France.

4. Department of Earth and Space Sciences, University of California, Los Angeles, Los Angeles, CA, United States.

**Body:** Interferometric synthetic aperture radar data are used to map the interseismic velocity field along the left-lateral Haiyuan fault system (HFS), at the north-eastern boundary of the Tibetan plateau. Two M~8 earthquakes ruptured the HFS in 1920 and 1927, but its 150 km-long central section, known as the Tianzhu seismic gap, remains unbroken since ~1000 years.

The Envisat SAR data, spanning the 2003-2009 period, cover ~600000 km-square along three descending and two ascending tracks. Interferograms are processed using an adapted version of ROI\_PAC, following a Small Baseline approach. Stratified tropospheric delays are empirically corrected, together with orbital residuals. Mean LOS velocity maps and phase range change increments are computed using a constrained time series analysis, after selection of interferograms with low residual atmospheric noise. A dominant left-lateral motion is observed across the HFS, as well as a narrow, 35 km-long zone of high velocity gradient across the fault in between the Tianzhu gap and the 1920 rupture. The inversion of average LOS velocity maps for shallow slip rate distribution reveals aseismic slip in between two fully locked segments. The creep rate is ~5 mm/yr in average, on the same order as the estimated loading rate at depth, suggesting no stress increase on the LHS segment. Still, local fault patches exhibit higher average creep rates, up to 8 mm/yr, revealing creep bursts.

We further explore the temporal fluctuations of the aseismic slip by smoothing the phase range change increments, applying a Gaussian temporal filter to minimize the effects of temporally uncorrelated turbulent atmospheric noise. Surface creep shows a rate increase between 2006 and 2007 up to 9-10 mm/yr locally. We model the temporal variations of the aseismic slip along the fault at depth adapting the Principal Component Analysis Inversion Method to our case study.

We finally analyse the relationships between the space and time evolution of the surface aseismic slip and the surface fault geometry, revealing a direct control of the fault roughness on the creep behavior.

## The evolution of fabric with displacement in natural brittle faults

*S. Mittempergher*<sup>1, 2</sup>; *G. Di Toro*<sup>1, 3</sup>; *J. Gratier*<sup>2</sup>; *S. Aretusini*<sup>1</sup>; *A. Boullier-Bertrand*<sup>2</sup>;

1. Department of Geosciences, University of Padova, Padova, Italy.

2. ISTerre, Grenoble, France.

3. INGV, Rome, Italy.

**Body:** In experiments performed at room temperature on gouges, a characteristic clast size distribution (CSD) is produced with increasing strain, and shear localization is documented to begin after few millimetres of sliding. But in natural faults active at depth in the crust, mechanical processes are associated with fluid-rock interactions, which might control the deformation and strength recovery. We aim to investigate the microstructural, geochemical and mineralogical evolution of low-displacement faults with increasing shear strain. The faults (cataclasite- and pseudotachylite-bearing) are hosted in tonalite and were active at 9-11 km and 250-300°C.

The samples were collected on a large glacier-polished outcrop, where major faults (accommodating up to 4300 mm of displacement) exploit pre-existing magmatic joints and are connected by a network of secondary fractures and faults (accommodating up to 500 mm of displacement) breaking intact tonalite. We performed optical and cathodoluminescence (CL) microscope, Scanning Electron Microscope (SEM), Energy Dispersive X-ray Spectroscopy (EDS), Rietveld X-Ray Powder Diffraction and microprobe chemical analysis in deformation zones of secondary faults with various offsets in order to evaluate the transfer of chemical species between dissolution zones and protected zones. Image analysis techniques were applied on SEM-BSE and optical microscope images to compute the CSD in samples, which experienced an increasing amount of strain.

The secondary fractures are up to 5 mm thick. Within the first 20 mm of displacement, shear localizes along Y and R1 surfaces and a cataclastic foliation develops. The CSD evolves from a fractal dimension D of 1.3 in fractures without visible displacement to values above 2 after the first 500 mm of displacement. Chemical maps and CL images indicate that the foliation in cataclasite results from the rotation and fragmentation of clasts, with dissolution of quartz and passive concentration of Ti oxides and titanite in the foliation planes. The cataclasites are cemented by pervasive precipitation of K-feldspar plagues and idiomorphic, randomly oriented, epidote and chlorite.

We conclude that the textures of these small displacement (< 500 mm) faults are controlled by brittle processes (fracture propagation and cataclastic comminution) similar to those reproduced in friction experiments performed on granite gouge (e.g., Beeler et al., 1996; Logan, 2007). Then progressively, stress driven fluid-rock reactions develop as fracturing and grain size reduction allows the kinetics of these reactions to be more efficient and fracture interconnection allows fluid infiltration. Healing of microfractures and fault rock cementation caused a rapid postseismic recovery of fault strength.

### References

Beeler, N.M., Tullis, T.E., Blanpied, L., Weeks, J.D., 1996. Frictional behaviour of large displacement experimental faults. *Journal of Geophysical Research* 101, B4, 8697-8715.

Logan, J.M., 2007. The progression from damage to localization of displacement observed in laboratory testing of porous rocks, in Lewis, H., and Couples, G.D. (eds.) *The relationship between damage and localization*. Geological



Final ID: GP23B-04

### Zonal shear and super-rotation in a magnetized spherical Couette flow experiment

*D. Brito*<sup>1</sup>; *T. Alboussière*<sup>3</sup>; *P. CARDIN*<sup>2</sup>; *N. Gagnière*<sup>2</sup>; *D. Jault*<sup>2</sup>; *P. La Rizza*<sup>2</sup>; *J. Masson*<sup>2</sup>; *H. Nataf*<sup>2</sup>; *D. Schmitt*<sup>2</sup>;

1. Université de Pau et des Pays de l'Adour , Laboratoire des Fluides Complexes et leurs Réservoirs, CNRS, Pau, France.

2. Université Joseph-Fourier, ISTERRE, CNRS , Grenoble, France.

3. Université de Lyon, Laboratoire de Sciences de la Terre, CNRS, Lyon, France.

**Body:** We present measurements performed in a spherical shell

filled with liquid sodium, where a 74 mm-radius inner sphere is rotated while a 210 mm-radius outer sphere is at rest.

The inner sphere holds a dipolar magnetic field and acts as a magnetic propeller when rotated. In this experimental set-up called DTS, direct measurements of the

velocity are performed by ultrasonic Doppler velocimetry.

Differences in electric potential and the induced magnetic field are also measured to characterize the

magnetohydrodynamic flow. Rotation frequencies of the inner sphere are varied between -30 Hz and +30 Hz, the magnetic Reynolds number based on measured sodium velocities

and on the shell radius reaching to about 33. We have investigated the mean axisymmetric part of the flow, which consists of differential rotation. Strong super-rotation of the fluid with respect to the rotating inner sphere is directly measured. It is found that the organization of the mean flow does not change much throughout the entire range of parameters covered by our experiment.

The direct measurements of zonal velocity give a nice illustration of Ferraro's law of isorotation in the vicinity of the inner sphere where magnetic forces dominate inertial ones. The transition from a Ferraro regime in the interior to a geostrophic regime, where inertial forces predominate, in the outer regions has been well documented.

It takes place where the local Elsasser number is about 1.

A quantitative agreement with non-linear numerical simulations is obtained when keeping the same Elsasser number.

The experiments also reveal a region that violates Ferraro's law just above the inner sphere.

Final ID: S24A-03

**Observations of non-linear behavior of seismic speed at low strain rate (*Invited*)**

*M. Campillo*<sup>1</sup>; *L. Retailleau*<sup>2, 1</sup>; *D. N. Rivet*<sup>1</sup>; *G. Hillers*<sup>1</sup>; *L. A. Rivera*<sup>2</sup>; *T. Nishimura*<sup>3</sup>; *K. Ma*<sup>4</sup>;

1. CNRS ISTERre, Univ Joseph Fourier, Grenoble, France.
2. EOST, Université de Strasbourg, Strasbourg, France.
3. Department of Geophysics, Tohoku University, Sendai, Japan.
4. Institute of Geophysics, National Central University, Chung-Li, Taiwan.

**Body:** We use ambient noise cross correlations to monitor slight changes in seismic velocities. The analysis of the records during a M7.5 slow slip event in the Mexican subduction zone suggests that the observed velocity change could be related with the volumic strain rate (Rivet et al., 2011). This observation is surprising when considering the level of strain rate, of the order of  $10^{-12}$ /s. At the same time the strain change itself is of the order of  $10^{-6}$ , which is above the threshold observed in laboratory experiments to detect non-linear effects on seismic speed (Johnson and Sutin, 2005).

Since the level of strain rate produced by tides is of the same order than the one associated with the slow slip event, we measure the differences between periods of high and low tidal strain, or strain rate, with ambient noise recordings at depth. Our data have been collected by 6 seismometers at about 1km depth from the Taiwan Chelungpu-fault Drilling Project (Ma et al., 2006), located in the active fault zone ruptured in the 1999 Chi-chi quake. Synthetic tidal strains, including oceanic loading, were modeled using GOTIC 2 codes and validated by comparison of gravity observations at a broad band station in the region of the borehole. We found no measurable difference of seismic velocity between periods of high and low tidal strain. On the contrary, we detect relative velocity changes between periods of high absolute values of strain rate and of constant strain. The amplitude of the relative velocity change is of the same order than in the case of the slow slip event, that is  $10^{-3}$ . These results suggest that the seismic velocity changes at short time scales and that the changes are correlated with strain rate rather than strain in the cases studied here. Note that the strain change produced by tides ( $10^{-8}$ ) is below the non-linear threshold observed in laboratory experiments.

Final ID: GP24B-04

reconstructing the geomagnetic field over the observatory era with a Bayesian approach (*Invited*)

N. Gillet<sup>1</sup>; D. Jault<sup>1</sup>; C. C. Finlay<sup>2</sup>;

1. ISTERre, Grenoble, France.

2. ETH, Zurich, Switzerland.

**Body:** More than one decade of global coverage geomagnetic data is now available from low-orbiting satellites. It has brought unprecedented constraints about the time changes of the Earth's magnetic field, enhancing the presence of interannual variations. Underlying physical processes must be investigated over longer series, such as that provided by ground observatories for the past century. However, all field models have been up to now based on regularization techniques that prevent the occurrence of rapid changes when less data are available. This process can result in biases when inverting sequentially core flow models from geomagnetic field models.

Here we depart from the regularization process to reconstruct the field evolution over the observatory era.

We deduce the prior covariance properties (variance and time correlation function as a function of harmonic degree) of the field model from the statistics of satellite field models. The posterior covariance matrix is then used to build an ensemble of field models that both fit geomagnetic data and satisfy the required covariance properties.

Final ID: S24A-06

**Locating a small change in a multiple scattering environment.**

*T. Planes*<sup>1</sup>; *E. F. Larose*<sup>1</sup>; *V. Rossetto*<sup>2</sup>; *L. Margerin*<sup>3</sup>;

1. ISTerre, CNRS & Université Joseph Fourier, Grenoble, France.
2. LPMMC, CNRS & Université Joseph Fourier, Grenoble, France.
3. IRAP, CNRS & Université Paul Sabatier, Toulouse, France.

**Body:** We present an imaging technique allowing locating a small perturbation appearing in a multiple scattering environment. This technique is based on the direct dependence in space and time of the coda decorrelation resulting from the apparition of a supplementary scatterer, which one wishes to image. The inverse problem solution – the location of the defect – is obtained using a maximum likelihood computation. The LOCADIFF technique has been applied to locate a millimeter change in concrete using ultrasounds with a precision of the order of one centimeter [Larose et al., Appl. Phys. Lett. 2010]. The size of the defect is comparable to that of the heterogeneities constituting the sample. We are currently working on a similar technique to locate small velocity perturbations in heterogeneous media, with potential applications on monitoring volcanoes and active faults.

Final ID: S24A-07

## Using Diffuse Field Theory to Interpret the H/V Spectral Ratio from Earthquake Records in a Mexico City site

*V. Salinas*<sup>1</sup>; *F. Luzón*<sup>2</sup>; *F. J. Sanchez-Sesma*<sup>4</sup>; *H. Kawase*<sup>3</sup>; *S. Matsushima*<sup>3</sup>; *M. Suárez*<sup>4</sup>; *A. Cuéllar*<sup>6</sup>  
; *D. N. Rivet*<sup>5</sup>; *M. Campillo*<sup>5</sup>;

1. ETCG, Universitat Politècnica de Catalunya, Barcelona, Barcelona, Spain.
2. Física Aplicada, Universidad de Almería, Almería, Almería, Spain.
3. DPRI, Kyoto University, Uji, Kyoto, Japan.
4. Instituto de Ingeniería, Universidad Nacional Autónoma de México, Coyoacán, México DF, Mexico.
5. Institut des Sciences de la Terre, Université Joseph Fourier, Grenoble, Grenoble, France.
6. Centro de Instrumentación y Registro Sísmico, A. C., Del. Benito Juárez, México DF, Mexico.

**Body:** It has been recently demonstrated that averaging the autocorrelations of ground motions within a diffuse field lead to the imaginary part of the corresponding Green's functions. This diffuse field assumption (DFA) is at the core of the proposed explanation for the microtremor H/V spectral ratio. An application was completely developed for a layered medium (Sánchez-Sesma et al., 2011). On the other hand, for sufficiently deep sources producing almost no surface waves at a 1D configuration, the 1D-DFA allows to relate the average H/V spectral ratio from earthquakes in terms of 1D Green's functions (Kawase et al., 2011).

In this work we consider earthquake data recorded at the Cibeles station belonging to the Mexico City Accelerometric Network. This site is in very soft ground and more than one hundred earthquakes of various magnitudes and locations have been recorded there between 1996 and 2008. A priori we did not know if the set of records could be regarded as realizations of a diffuse field. In order to explore the characteristics of this data set, we did the averages of the autocorrelations of windows for these earthquakes. We consider various receiver-source configurations in terms of theoretical incidence angle and consider separately, when that was possible, P, S and Coda waves.

We made a parametric study considering the various attributes for this data set. Although we expected significant differences for the, say, S and Coda windows, we found instead remarkable consistency of H/V for the various combinations, perhaps with some deviations for P windows. Moreover, we found that the H/V of the recorded data matches very well with the theoretical spectra computed using the imaginary part of 3D Green's function for the standard layered structure of the site. This fact strongly suggests that, thanks to multiple scattering, the seismic fields from various earthquakes can be regarded as realizations of 3D diffuse fields. Comparisons are provided for microtremor measurements as well.

We discuss the implications of these results for structure inversion in Mexico City.

Final ID: A31A-0043

### Studying of Infrasonic Sources Generated by the Swell

*M. Landès*<sup>1</sup>; *L. Ceranna*<sup>2</sup>; *A. LE PICHON*<sup>1</sup>; *G. Hillers*<sup>3</sup>; *R. S. Matoza*<sup>4</sup>;

1. CEA, DAM, DIF, Arpajon, France.

2. BGR, Hannover, Germany.

3. ISTERRE, Grenoble, France.

4. Scripps Institution of Oceanography, Institute of Geophysics and Planetary Physics, La Jolla, CA, United States.

**Body:** Although currently not fully established, the infrasound network of the International Monitoring System (IMS) of the Comprehensive Nuclear-Test-Ban Treaty organization allows studies on a global scale, dealing with various topics like detection capability simulation, continuous monitoring of the atmosphere, or atmosphere/ocean interface modeling. The background noise plays a dominant role in the selection of signals of interest especially near 0.2 Hz where the noise amplitude increases due to microbarom signals. The study of microbarom sources therefore helps improving the detection of nuclear explosions and volcanic eruptions, and allows microbarom detections to be used as continuous sources for monitoring atmospheric dynamics.

Continuous infrasound monitoring from 2006 to 2010 provides monthly localizations of microbarom sources. These results, obtained with a multi-year averaging approach and a simple cross-bearing method, exhibit clear seasonal trends consistent with annual climate variations. At regional scales, the interpretation of microbarom observations at a single station remains challenging. For few IMS stations, we try to characterise microbarom detections using a source model derived from wave interaction maps and the ECMWF wind model. This attempt highlights uncertainties when comparing microbarom modeling with observations. However, both statistical and quantitative approaches for microbarom studies provide new insights on quantitative relationships between infrasonic observables, atmospheric specifications, and interactions between atmosphere and ocean.

Final ID: ED31A-0727

## THE LITHOSPHERIC STRUCTURE OF THE WESTERN TURKEY AND AEGEAN REGION

*T. Afacan Ergun*<sup>1</sup>; *H. Karabulut*<sup>1</sup>; *A. Paul*<sup>2</sup>;

1. Bogaziçi University, Kandilli Observatory and Earthquake Research Institute, Istanbul, Turkey.

2. Laboratoire de Géophysique Interne et Tectonophysique (LGIT), Grenoble, France.

**Body** : A broad-scale seismological experiment, SIMBAAD (Seismic Imaging Beneath the Aegean-Anatolia Domain), is performed in the Aegean-Anatolia region. The objective of the project is to investigate the crustal and mantle structure beneath Western Turkey, the Aegean Sea, and continental Greece. This tectonically very active region has experienced a variety of geodynamic processes and its geology and kinematics have been extensively studied. It is thus a good place to test competing hypotheses on how the surface kinematics is related to mantle structure and dynamics.

In the spring of 2007, we installed a temporary network of 33 broadband stations in Turkey, Greece, and S-Bulgaria for 2- year duration. It complemented the permanent broadband networks (~90 stations) with an inter-station spacing of ~100 km in the region. The experiment also included 2 north-south profiles of more densely-spaced stations (~15 km) crossing Western Anatolia at 18°E and 31.5°E.

We performed receiver function analysis on the western transect of 430km in length including 26 stations. Over 60 teleseisms (30° to 95° distance) were used in the analysis and more than 2000 receivers functions were computed. We determined  $V_p/V_s$  ratios using H-k stacking method and applied common conversion point stacking to receiver functions of the N-S linear array. The results indicates an average Moho depth of 30 km with negligible variations under the major grabens and core complexes (e.g. Menderes massif).

Final ID: EP31E-0863

**Scaling Analysis of Deformation Field within Granular Materials: application to Strain Localization.**

*F. Gimbert*<sup>1,3</sup>; *D. Amitrano*<sup>1</sup>; *G. Combe*<sup>2</sup>; *J. Weiss*<sup>3</sup>;

1. ISTERre, Grenoble, France.
2. 3S-R, Grenoble, France.
3. LGGE - CNRS/UJF, Grenoble, France.

**Body:** Discrete element method (DEM) simulations using periodic boundary conditions and molecular dynamics are conducted on a frictional granular media. Two dimensional strain or stress controlled biaxial tests are carried out on an assembly of circular particles interacting via elastic contacts and Coulomb friction. The spatial correlations that take place within the deformation field along the loading path are tracked by a scaling analysis of the continuous strain rate field. This method allows us to discuss the degree of strain localization occurring throughout the test. The analysis of the correlation length in the early stages of macroscopic deformation leads to the identification of two distinct behaviors. First, a divergence of the correlation length on the first deformation invariant, i.e. the divergence, is reported at the onset of macroscopic dilation. This suggests an interpretation of the contraction peak as a critical point. Secondly, an increase of the correlation length on the second deformation invariant, i.e. the shear, is also observed before the peak load. However, saturation remains on the scaling law. We argue that this second behavior is associated to macroscopic shear banding: our analysis accurately gives its outbreak on the stress versus strain curve. Finally, a dependence of the correlation length as a function of the deformation window considered is reported. This shows that scaling properties within the deformation field emerge from long range interactions within an assembly of rigid frictional particles.

**Experimental lighting of water velocity around macropores in a porous media**

*L. Lassabatere*<sup>1</sup>; *T. Lenoir*<sup>2</sup>; *P. Peyneau*<sup>2</sup>; *E. Lamy*<sup>3</sup>; *B. Bechet*<sup>2</sup>; *R. Angulo-Jaramillo*<sup>1</sup>; *A. Simionovici*<sup>4</sup>; *A. Manceau*<sup>5</sup>;

1. LEHNA-IPE, UMR 5023, University of Lyon, ENTPE, Vaulx en Velin, France.
2. LUNAM, IFSTTAR, Nantes, France.
3. Chemical Engineering, Université de Technologie de Compiègne, Compiègne, France.
4. D Laboratoire de Géologie de Lyon : Terre, Planètes, Environnement, Lyon, France.
5. ISTerre - Université J. Fourier, Grenoble, France.

**Body:** In recent years, much attention and concern have been given to problems associated with contaminant transport on both surface and ground-water systems. Through the vadose zone, it is difficult to predict water and solute transport due, in part, to the structure heterogeneity of natural soil formations. The difficulty is compounded in soils that contain preferential flow path due to the presence of cracks, structural peds, wormholes, and root channels. The importance of macropore flow for solute transport has been demonstrated by means of breakthrough experiments on undisturbed soil columns amended with artificial macropores. Lamy et al. (2009) clearly stated that macropores enhanced solute transport leading to an earlier breakthrough with a substantial tailing at the outlet of the columns. These authors also showed that the experimental breakthrough curves could not be properly modelled unless flow was regarded as enhanced in the matrix surrounding the macropore. Yet, they did not provide any experimental evidence for such hypothesis; and very few studies focused on such evidence. The objective of this work is to give experimental evidence to verify this statement. Columns, 5 cm in diameter and 10 cm in length, were made of a silt/cement and of a sand/cement mix with a thin stick located along their vertical axis. After cementation, the stick was removed, leading to a continuous macropore of 500 µm in radius through the whole system. An iodine solution has been injected through these columns and then, they have been scanned using the 8.3.10 beamline of the Advanced Light Source, at the Lawrence Berkeley National Laboratory, in order to obtain the 3D image-distribution of iodine. The experimental data reveal the presence of iodine in a significant part of the matrix surrounding the macropore and enlightens the extension of the preferential flow around the macropore. . Such experimental data clearly underscores the need to consider enhanced flow in a portion of the surrounding matrix as well. This is of great interest in regards to the proper choice of conceptual and quantitative modelling of coupled macropore flow and pollutant transfer.

Lamy E., Lassabatere L., Bechet B., Andrieu H. 2009. Modeling the influence of an artificial macropore in sandy columns on flow and transfer. *Journal of hydrology*, 376, 392-402. (doi:10.1016/j.jhydrol.2009.07.048).

Final ID: S31C-2251

**Do variations of the ambient noise wavefield reflect on measured seismic velocity changes?**

*C. Hadziioannou*<sup>1</sup>; *E. F. Larose*<sup>2</sup>; *P. Roux*<sup>2</sup>; *M. Campillo*<sup>2</sup>; *J. M. Wassermann*<sup>1</sup>; *H. Igel*<sup>1</sup>;

1. LMU, Munich, Germany.

2. ISTerre, Grenoble, France.

**Body:** One way of monitoring changes in seismic wave velocities is by following short-term variations in noise correlation functions calculated on short time windows. However, difficulties may arise when the spatial distribution of noise sources evolves with time as well.

The relationship between the measured seismic velocity fluctuations and the time-evolution of the spatial distribution of the noise wavefield is investigated through beamforming analysis. We show why it is important to monitor the evolution of the ambient noise wavefield when one wants to assess the reliability of measurements of velocity changes.

Finally, a way of determining a noise source orientation using only a co-located measurement of translational and rotational motion is presented.

Final ID: S31C-2259

**Using curvelet filter to improve the temporal resolution of seismic waves speed changes measured from ambient noise correlations.**

*L. Stehly*<sup>1</sup>; *B. FROMENT*<sup>2</sup>; *M. Campillo*<sup>2</sup>; *J. Chen*<sup>3</sup>; *Q. Liu*<sup>3</sup>;

1. Géoazur, Observatoire de la Côte d'Azur, Sophia Antipolis, France.

2. ISTerre - Institute de Science de la Terre, Université Joseph Fourier, Grenoble, France.

3. State Key Laboratory of Earthquake Dynamics, Institute of Geology, China Earthquake Administration, Beijing, China.

**Body:** The aim of this work is to improve the temporal resolution of velocity change observations measured from ambient noise correlations.

Following the work of Chen et al, 2010, we study the seismic wave speed changes associated with the Mw 7.9 Wenchuan earthquake using 21 broadband stations distributed across the fault activated during the earthquake.

We take advantage of the properties of the curvelet transform, a 2D transform that provides an optimally sparse representation of 2D Green functions in smooth medium, to filter out the noise out of the correlations while keeping the signal corresponding to the green function.

The use of these curvelet denoising filters allows us to speed up the convergence of the noise correlations toward the Green function, and to improve the reconstruction of coda waves. It is then possible to get a temporal resolution of less than one day, and to discriminate co-seismic and post-seismic velocity changes.

**Deformation cycle of the Grímsvötn sub-glacial volcano, Iceland, measured by GPS**

*E. C. Sturkell*<sup>1, 2</sup>; *F. Sigmundsson*<sup>2</sup>; *P. Einarsson*<sup>3</sup>; *S. Hreinsdóttir*<sup>3</sup>; *T. Villemin*<sup>4</sup>; *H. Geirsson*<sup>5</sup>; *B. G. Ófeigsson*<sup>6</sup>; *F. Jouanne*<sup>7</sup>; *H. Björnsson*<sup>3</sup>; *G. B. Gudmundsson*<sup>6</sup>; *F. Pálsson*<sup>3</sup>;

1. University of Gothenburg, Dept of Earth Sciences, Gothenburg, Sweden.
2. Nordic Volcanological Center, Institute of Earth Sciences, University of Iceland, Reykjavik, Iceland.
3. Institute of Earth Sciences, University of Iceland, Reykjavik, Iceland.
4. Laboratoire de Géodynamique des Chaînes Alpines UMR 5025, Université de Savoie, Le Bourget du lac, France.
5. Department of Geosciences, The Pennsylvania State University, University Park, PA, United States.
6. The Icelandic Meteorological Office, Reykjavik, Iceland.
7. Laboratoire de Géodynamique des Chaînes Alpines, Université de Savoie, Le Bourget du lac, France.

**Body:** The subglacial Grímsvötn volcano in Vatnajökull ice cap erupted in 1998, 2004, and 2011. We present results of Global Positioning System (GPS) geodetic measurements since 1997 conducted at one site on the volcano's caldera rim, which protrudes through the ice cap. The volcano contains a complex of three calderas (<12 km<sup>2</sup> each). The observed displacement can be attributed to several processes: i) transport of magma in and out of a shallow chamber under the center of a caldera complex (inflation, deflation, accompanied by in- and outward horizontal displacements), ii) isostatic uplift due to gradual thinning of the ice cap, iii) annual variation in snow load, iv) crustal plate movements. Annual GPS measurements started after the 1998 eruption and a continuous GPS-monitoring station has been operative shortly before the 2004 eruption. During inflation periods the vertical displacement is a joint result of a glacial isostatic adjustment due to thinning of the glacier and inflow of magma to a shallow magma chamber, while the horizontal displacement component is predominately attributed to magma pressure changes. The horizontal displacement of the GPS-site on the caldera rim is directed outward during inflation and inward (directly opposite) accompanying the eruptions. This pattern has been repeated for each eruption cycle, pointing to location of one and the same magma chamber in the center of the caldera complex. Erupting vents in 1998, 2004 and 2011 were located at the foot of the southern Grímsvötn caldera rim. The earthquake pattern was similar prior to the two most recent eruptions: a slow increase in number of events during the years before the eruptions and practically none following the eruptions. The continuous GPS data after the eruption in 2011 suggest a fast pressure recovery of the shallow magma chamber similar to that following the 1998 and 2004 eruptions, although the 2011 eruption is the best observed. The regularity of the crustal deformation and the earthquake pattern prior to the past two eruptions led to both successful long- and short-term predictions and warning of the events. Grímsvötn volcano has shown to be in a state of continuous magma accumulation at shallow depths that results in eruptions when the strength of the crust is overcome by the magma pressure.

Final ID: S31G-07

**Slow slip events and strain accumulation in the Guerrero gap, Mexico.**

*F. Cotton*<sup>1</sup>; *M. Radiguet*<sup>1</sup>; *M. M. Vergnolle*<sup>2</sup>; *M. Campillo*<sup>1</sup>; *A. Walpersdorf*<sup>1</sup>; *N. Cotte*<sup>1</sup>; *V. Kostoglodov*<sup>3</sup>;

1. ISTERre, Grenoble, France.
2. GeoAzur, Nice, France.
3. UNAM, Mexico City, Mexico.

**Body:** GPS time series in Guerrero (Mexico) reveal the existence of large slow slip events at the boundary between the Cocos and North America plates. In this study, we examine the last three slow slip events that occurred in 2002, 2006 and 2009-2010, and their impact on the strain accumulation along the Guerrero subduction margin. GPS displacements are inverted to retrieve the slip distribution during each SSE, and the inter-SSE coupling of the subduction interface. The three analyzed SSEs have equivalent moment magnitudes between 7.5 and 7.65, their lateral extension is variable, and they all show important slip in the Guerrero seismic gap. During the inter-SSE epochs the interplate coupling is high in the area where slow slip consequently occurs. In the Guerrero gap, the shallow portion of the plate interface, from the trench to the coast is weakly coupled. The average slip deficit accumulated in the Guerrero gap over a period of 12 years, corresponding to three cycles of SSEs is only 1/4 of the slip deficit accumulated on both sides of the gap. Moreover, the regions of large slip deficit coincide with the rupture areas of recent large earthquakes. We conclude that the slow slip events in the Guerrero gap release a significant part of the strain accumulated during the inter-SSE period, and probably increase the recurrence time of large subduction thrust earthquakes in the Guerrero gap.

**New Results of Studies of Slow Slip Events and Nonvolcanic Tremor in the Guerrero Seismic Gap, Mexico (G-GAP project)**

*V. Kostoglodov*<sup>1</sup>; *D. Zigone*<sup>2</sup>; *A. L. Husker*<sup>1</sup>; *M. Campillo*<sup>2</sup>; *D. N. Rivet*<sup>2</sup>; *N. M. Shapiro*<sup>3</sup>; *M. Radiguet*<sup>2</sup>; *W. Frank*<sup>2</sup>; *G. Hillers*<sup>2</sup>; *N. Cotte*<sup>2</sup>; *G. Cougoulat*<sup>2</sup>; *J. S. Payero*<sup>1</sup>; *V. Cruz-Atienza*<sup>1</sup>;

1. Seismology, UNAM, Instituto de Geofísica, Mexico City, DF, Mexico.

2. CNRS ISTERre, Univ Joseph Fourier, Grenoble, France.

3. Institut de Physique du Globe de Paris, Paris, France.

**Body:** The Guerrero seismic gap located in the Central Mexico subduction zone is a hot area of intensive study as it apparently has accumulated, for the last 100 years, sufficient elastic strain to be released in Mw~7.8-8.0 earthquake. Since its installation, the permanent GPS network in Mexico detected 4 large Slow Slip Events (SSE) with a periodicity of about 4 years and possibly smaller and more frequent SSEs. Comprehensive analysis and modeling of GPS data revealed a very important strain release by those SSE in the gap. It comes out that the interplate coupling and elastic strain accumulation in the seismogenic zone of the Guerrero gap is much lower than in the neighboring segments of the zone, which suffer large subduction thrust earthquakes more frequently.

Seismic networks in Guerrero are detecting Non-Volcanic tremors (NVT) with different characteristics and locations. Low energy NVT is occurring almost continuously at a distance of ~215 km from the trench. During large SSEs, the duration and frequency of the NVT bursts increased and low energy bursts are also observed as close as ~150 km to the trench. Some NVT bursts may coincide with smaller SSEs, extending ~180 km to ~220 km from the trench with durations of a few weeks. Our observations indicate that some parts of the NVT in Guerrero can be associated with the Low-Frequency Earthquakes (LFE). However, the amount of identifiable LFEs is very small.

We also observed strong triggering of the NVT activity by teleseismic waves after Maule, Chile 2010 earthquake that overlapped with the latest 2009-2010 strong SSE in Guerrero. Conversely the Great Tohoku 2011 earthquake that occurred after the termination of this SSE did not produce any noticeable tremor excitation in Guerrero.

### Geophysical monitoring of ground moisture within a clayey landslide

*G. Bièvre*<sup>1,2</sup>; *L. Oxarango*<sup>3</sup>; *D. Jongmans*<sup>2</sup>; *S. Grangeon*<sup>2</sup>; *C. Hung*<sup>4</sup>; *S. Palma-Lopes*<sup>5</sup>;

1. Laboratoire de Lyon, CETE de Lyon, Lyon, France.
2. ISTerre, Université de Grenoble, Grenoble, France.
3. LTHE, Université de Grenoble, Grenoble, France.
4. Laboratoire d'Autun, CETE de Lyon, Autun, France.
5. IFSTTAR, Nantes, France.

**Body:** Ground moisture is a key-parameter to assess and monitor natural hazards like clayey landslides as well as the penetration depth of drought. Some geophysical techniques provide measurements of physical parameters which can be related to water content. This study aims at enhancing the knowledge about infiltration processes within these clayey levels and at determining the most appropriate geophysical method to monitor ground moisture within the first meters.

The study site is located in the French Alps, in a 300 km<sup>2</sup> area made of laminated clays and silts deposited within an ice-dammed lake. The glacier retreat (15ky ago) favoured the initiation of multiple landslides and 15% of the area is presently prone to landsliding with known dramatic issues (4 fatalities in 1994). The study site is part of a French national observatory (OMIV; [www-iglit.obs.ujf-grenoble.fr/observations/omiv/](http://www-iglit.obs.ujf-grenoble.fr/observations/omiv/)) and is equipped with permanent probes: Time Domain Reflectometry (TDR), ground temperature, pressure cells (for hydrostatic levels) and a meteorological station.

Volumetric water contents (VWC) of the first 5 m were determined at different periods of a year using electrical resistivity tomography (ERT) and neutron probe logging. ERT measurements were processed with a time-lapse inversion approach, using the first model as a starting model for further data, and then temperature-corrected. Laboratory calibration was conducted on controlled samples (VWC, density, temperature) for which the geometrical factor was numerically determined. Neutron and gamma probe measurements were conducted every 0.25 m with a Campbell probe or every 0.02 m with a prototype.

Results obtained from the three geophysical techniques are in good agreement and provide VWC between 20 and 45%. TDR measurements are in good agreement with meteorological and pressure data. They show that the first 2 m quickly react to rainfall and/or snow melt, but they only provide 1D vertically discontinuous information. Neutron logging, along with TDR, shows the presence of the water table at depth as well as 2 small perched water tables that were not previously detected. Vertical resolution is much higher than with TDR but still only provides 1D information. ERT 2D images present a VWC in the first 0.7 m which is underestimated as compared to other tools and which can be linked to a slightly varying lithology in this part. On another way, they reveal laterally heterogeneous resistivity (and, hence, VWC) which correspond to open fissures and which seem to correspond to preferential infiltration paths down to the water table. ERT images reveal heterogeneities, possibly linked to 3D effects which could alter VWC determination.

The results of the geophysical investigation point to a higher hydrogeological complexity than what was previously assumed and also indicate that the combination of the three techniques significantly enhance the understanding of the subsurface hydrogeological processes. Finally, it has been possible to highlight the main advantages and drawbacks of each technique in the aim of providing an efficient tool to monitor water content.

Final ID: T33F-2486

## Numerical Investigation of Weak Grains in Granular Shear Zones

*A. P. Rathbun*<sup>1</sup>; *F. Renard*<sup>1,2</sup>; *S. Abe*<sup>3</sup>;

1. ISTerre, University Joseph Fourier – Grenoble I & CNRS, Grenoble, France.

2. Physics of Geological Processes, University of Oslo, Oslo, Norway.

3. RWTH Aachen, Geologie-Endogene Dynamik, University of Aachen, Aachen, Germany.

**Body:** The role of frictionally weak particles is central in understanding various types of shear zones including faults, landslides and deformation in glacial till. All of these deformation zones contain a mixture of mineral phases and can include significant proportions of frictionally weak particles such as clay minerals and phyllosilicates. This observation was used, for example, to explain the weak frictional behavior of the San Andreas Fault. Understanding the role of these phases on overall fault strength and localization of shear is necessary to understand the generation of shear and earthquakes. Here, we use a 3D Discrete Element Method (DEM) numerical approach to investigate the role of weak particles on the overall frictional strength of a deforming shear zone. The DEM allows us to investigate the micromechanics of the shear zone by directly visualizing force chain formation, connectivity and destruction and also the distributed or localized nature of shear in the numerical experiment. The shear zone of our models is compared to standard laboratory friction experiments in which non-cohesive grains (fault gouge) are sandwiched between stiff walls and sheared. The gouge particles in our models range from 100 to 200  $\mu\text{m}$  in diameter with the normal stress held constant at 15 MPa. We vary the coefficient of friction between particles and mix frictionally strong and weak particles in different ratios. Additionally we investigate the shape of phyllosilicates and their role in localization of shear into plane by varying the shape of grains from spheres to platy grains. Our study provides some quantitative information on the proportion of weak particles necessary to significantly reduce the strength of a shear zone.

Final ID: V33A-2619

### Jet dynamics at Lone Star Geyser, Yellowstone National Park

*L. Karlstrom*<sup>1</sup>; *M. L. Rudolph*<sup>1</sup>; *J. Vandemeulebrouck*<sup>3</sup>; *F. Murphy*<sup>2</sup>; *S. Hurwitz*<sup>2</sup>; *M. Manga*<sup>1</sup>; *R. A. Sohn*<sup>4</sup>; *M. J. Johnston*<sup>2</sup>;

1. Earth and Planetary Science, UC Berkeley, San Francisco, CA, United States.
2. US Geological Survey, Menlo Park, CA, United States.
3. ISTERre, Universite de Savoie, Le Bourget du Lac Cedex, France.
4. Woods Hole Oceanographic Institution, Woods Hole, MA, United States.

**Body:** Geysers provide a natural laboratory to study multiphase eruption processes and the geophysical signals that can be measured before, during, and after an eruption. As part of a field study at Lone Star Geyser, Yellowstone National Park in September, 2010, we recorded multiple consecutive eruptions with visible and infrared video and an audio microphone. These measurements, along with water discharge measurements in outflow streams, allow us to constrain eruptive liquid and steam volumes and calculate aspects of jet dynamics and energetics. We perform Particle Image velocimetry (PIV) analysis of high-speed visible video images to extract maximum jet velocity and height throughout an eruption. We find that the time and frequency domain structure of maximum velocity is similar to that of median jet temperature and amplitude of acoustic emissions. We correlate visible and infrared video to estimate the mass fraction of steam versus liquid throughout an eruption, and use this to calculate an energy budget for the geyser. The clear transition from liquid to steam dominated flow during eruption is mirrored in the frequency domain, likely reflecting a shift in the sound speed of the mixture and a transition towards choked conditions during eruptions. However unsteadiness in the flow implies that this condition is not always met.

## Recent mechanical weakening of the Arctic sea ice cover as revealed from larger inertial oscillations. Observations and Analytical Modelling.

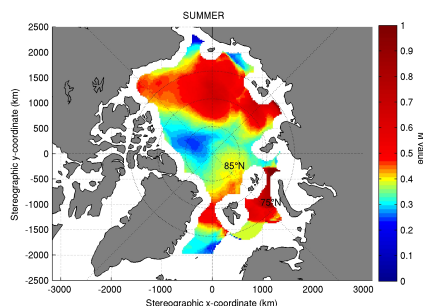
*F. Gimbert*<sup>1,2</sup>; *N. Jourdain*<sup>3</sup>; *D. Marsan*<sup>4</sup>; *J. Weiss*<sup>2</sup>; *B. Barnier*<sup>3</sup>;

1. ISTERre - CNRS/UJF, Grenoble, France.
2. LGGE - CNRS/UJF, Grenoble, France.
3. LEGI - CNRS/UJF, Grenoble, France.
4. ISTERre - CNRS/UJF, Le Bourget du Lac, France.

**Body:** An original method to estimate the degree of cohesiveness of the sea ice cover is developed from the analysis of oceanic and ice-tethered buoys inertial motion. A non-dimensional parameter  $M$  is defined from a spectral analysis in order to quantify the amplitude of the sea ice inertial oscillations. This parameter is used to investigate the sea ice mechanical properties. A strong seasonal dependence of the sea ice inertial oscillations magnitude is revealed, in agreement with the corresponding annual cycles of sea ice extent, concentration, thickness, advection velocity, and deformation rates. The spatial pattern of the sea ice inertial oscillations magnitude over the Arctic basin is also in agreement with the sea ice thickness and concentration patterns (see image). A significant pluri-annual evolution towards larger inertial oscillations magnitude in recent years is particularly remarkable since 1996-1997 and in the eastern Arctic regions where the sea-ice decline has been especially marked.

To quantitatively interpret variations of the inertial oscillations magnitude in term of mechanical behaviour of the ice cover, we propose a simple ocean boundary layer-sea ice coupled analytical model that we apply to the modelling of Arctic sea ice motion in the frequency domain. This simple model, where the sea ice mechanical response is simplified through the introduction of a linear internal friction term  $K$ , describes well the average sea ice motion from inertial motion to advection motion. In particular, it allows explaining the seasonal and regional dependence of Arctic sea ice inertial motion through an associated dependence of  $K$ .  $K$  is maximal for the thick multi-year ice pack in winter, and minimal in summer over a peripheral zone covered nowadays mainly by 1st-year ice. In addition, a significant decrease of  $K$  at least by a factor 2, i.e. a mechanical weakening of the sea ice cover, is observed for the period 1997-2008 compared to 1989-1996, for the entire Arctic in both seasons.

These results show that the regional, seasonal and pluri-annual variations of sea ice inertial motion observed initially are not only the trivial consequence of changes of the ice mass per unit area but are accompanied by a mechanical weakening of the sea ice cover.



Spatial pattern of inertial oscillation magnitude within the Arctic basin in summer.

Information on the Motions within the Earth's Core and on the Geomagnetic Field prior to Geomagnetic Data Inversion

*(Invited)*

*D. Jault*<sup>2, 1</sup>; *N. Gillet*<sup>1</sup>; *N. Schaeffer*<sup>1</sup>;

1. ISTERre, CNRS, Univ Grenoble, Grenoble Cedex 9, France.

2. Earth and Planetary Magnetism, ETH, Zürich, Switzerland.

**Body:** The classical procedure to calculate fluid motions at the Earth's core surface, evolving over the last  $10^2$  years, does not take adequately into account our uncertainties on the geomagnetic field and its temporal variations. Indeed, these calculations are usually achieved using unjustifiably regularized magnetic field models, which forgo rapid time variations and were the only ones available until recently. The usual hypotheses on the kinetic energy spectrum, that are made prior to core flow inversions, amount to heavily penalizing small-scale core flows. They appear also strikingly unrealistic, in the light of a recent estimation of the Earth's core magnetic energy. We adopt a different approach and base our discussion of the ratio between the kinetic and magnetic energy densities - as a function of the harmonic degree - on physical considerations.

For the largest length-scales, this ratio of energy densities probably does not exceed  $10^{-3}$ . We argue that it increases with the wavenumber up to a value of the order of 1 for the length-scale at which inertial and magnetic waves have similar periods. We find this description well supported by the results of some numerical investigations of the geodynamo equations. We thus deduce information on the kinetic energy spectrum that we can use as prior knowledge before calculating core flows. We can then rely on a newly calculated magnetic field model for the epoch 1900-2010 to determine quasi-geostrophic core flows as consistently as presently possible. Applying an ensemble technique, we are able to deal with the uncertainties on the magnetic field. We discuss to what extent the calculated flow models depend on the a priori information on the magnetic field time variability. Our choice of priors takes into account the recent discovery of rapid changes of the largest scales of the magnetic field in models derived from satellite data and the occurrence of geomagnetic jerks. Finally, we consider that such a discussion of the prior information on the magnetic and velocity fields is a prerequisite before renewed geomagnetic data assimilation attempts.

**Finding the buried memory of past earthquakes with geophysical, GPR-based paleoseismology**

*I. Manighetti*<sup>1,2</sup>; *S. Beaupretre*<sup>2</sup>; *S. Garambois*<sup>2</sup>; *J. Malavieille*<sup>3</sup>; *M. Chatton*<sup>3</sup>; *G. Sénéchal*<sup>4</sup>;

1. GEOAZUR-OCA-CNRS, Nice, France.
2. ISTERRE, Grenoble, France.
3. Geosciences Montpellier, Montpellier, France.
4. IPRA, Pau, France.

**Body:** We hypothesized that, in places where sedimentation and erosion compete at fast rates, part of the memory of past earthquakes on faults may be buried, hence hidden, in the first tens meters of the ground. We test that hypothesis on a fast slipping, large, strike-slip fault (Hope, New Zealand), at a site where marked alluvial conditions prevail (Terako). We first use LiDAR data to analyze the ground surface morphology of the 2 km<sup>2</sup> site at the greatest resolution. About twenty clear, distinct, morphological markers are observed –mainly alluvial terrace risers and small stream channels, all are laterally offset by the fault. The measured offsets range between 3 and 200 m, yet are discrete and showing several large slip gaps. The measurements are well-constrained and allow estimating the mean slip per event amplitude to  $3.9 \pm 1.4$  m, and the last earthquake slip to  $3 \pm 0.5$  m. About 10 past earthquakes are well documented in the surface data, while about 50 are requested to account for the 200 m largest cumulative slip. We then investigate the zone (on smaller area, 400 x 600 m<sup>2</sup>) with dense, pseudo-3D Ground Penetrating Radar (GPR) data. We measured 56, ~400 m-long, 5-10 m spaced GPR profiles (250 MHz), parallel to the fault and evenly distributed on either sides. Their analysis reveals the existence of several tens morphological markers buried in the first 3 m of the ground, most of them do not imprint the ground surface as they are blanketed with a 0.1-3 m-thick poorly reflective layer. A few buried markers exhibit however surface expressions. All buried markers are laterally offset by the fault. Based on a number of evidence, we interpret these buried markers as stream channels, most were decapitated by the repeated fault slips and abandoned. We measured ~50 lateral offsets in the buried channel network, almost three times more than at the surface. These offsets range between 2.5 and 106 m, as observed at the surface, yet provide a more continuous record of the fault slip. The similarity of the successive slip increments suggests a slip per event averaging  $3.9 \pm 1.9$  m, similar to that estimated from surface data. From the total 'surface and buried' offset collection, we infer that a minimum of 30 large earthquakes have broken the Hope fault at the Terako site in the last 5 kyrs, with an average slip per event of  $3.8 \pm 1.3$  m, an average recurrence time of 100-250 yrs, and a likely magnitude of at least Mw 7.2-7.7. The last major earthquake likely occurred at  $1875 \pm 15$  AD, in agreement with previous suggestions. Our study therefore confirms that part of the memory of past earthquakes may indeed reside in the first tens meters of the ground, where it may be explored with a novel type, geophysical and GPR-based, paleoseismology. We emphasize that developing such a new paleoseismology will provide a rich information complementary to surface observation, and help documenting the past earthquakes on faults.

## A New Design for Digital Elevation Models of Bedrock Underlying Ice Sheets

*A. Drouet*<sup>2</sup>; *G. Durand*<sup>2</sup>; *F. Gillet-chaulet*<sup>2</sup>; *E. Le Meur*<sup>2</sup>; *J. Braun*<sup>6</sup>; *M. Sacchetti*<sup>2</sup>; *D. A. Young*<sup>4</sup>; *D. Blankenship*<sup>4</sup>; *J. Greenbaum*<sup>4</sup>; *A. Wright*<sup>7</sup>; *E. J. Rignot*<sup>5, 3</sup>; *Y. Gim*<sup>3</sup>; *J. Mouginot*<sup>5</sup>; *D. Kirchner*<sup>1</sup>;

1. University of Iowa, Iowa, IA, United States.
2. LGGE, Saint Martin D'Hère, France.
3. JPL, Pasadena, CA, United States.
4. UT, Austin, TX, United States.
5. UC, Irvine, CA, United States.
6. ISTERRE, Saint Martin D'Hères, France.
7. University of Edinburgh, Edinburgh, United Kingdom.

**Body:** Proper knowledge of bedrock topography is an important prerequisite in order to model ice sheet behavior and estimate their future contribution to sea level rise. Today, 5-km resolution Digital Elevation Models are commonly used by modelers to obtain bedrock elevation on their grid nodes.

This chosen resolution is questionable since most of the ice outflow goes through outlet glaciers whose size is of a similar order of magnitude, leading modelers to refine their grid with maximum mesh resolution of the order of 100 m.

In this study, we show that for modeling purposes, using current 5-km regular DEMs requires an 'undermeshing' interpolation that can locally lead to up to 100% relative error on the ice thickness value as well as opposite directions of the bedrock slope. We here propose to modify the way DEMs are usually processed. This paradigm shift consists of moving from static DEMs with interpolated data on a regular mesh to more flexible ones that return a direct interpolation at the precise locations required by the user mesh. An illustration with the Astrolabe drainage basin (East Antarctica) is described, based on intensive ice thickness radar measurements that have been performed over the last 3 years. Eventually, an application under the form of a web interface is proposed to demonstrate the feasibility of such a procedure.

Final ID: EP41B-0610

## Large Nd-Hf isotopic decoupling in Himalayan River Sediments

*M. Garçon*<sup>1</sup>; *C. Chauvel*<sup>1</sup>; *C. France-Lanord*<sup>2</sup>;

1. ISTERre, Grenoble, France.

2. CRPG-CNRS, Nancy, France.

**Body:** Nd isotopic compositions of river sediments are widely used to trace sediment provenance in the Himalayan mountain range. In contrast, Hf isotopic compositions are not used even though they are excellent proxies to record the history of continental areas (Hawkesworth and Kemp, *Chem. Geol.* 226, 2006). Here, we focus on the Hf isotopic message carried by Himalayan river sediments and combine it to the more classical Nd isotopes to better understand the behavior of the two systems during erosion.

We report Nd-Hf isotopic compositions of bedloads and suspended loads sampled at different depths in the Narayani River in Nepal (upstream of the Ganga floodplain), in the Ganga River in Bangladesh (downstream of the Ganga floodplain) and in the Yamuna River, a major tributary of the Ganga in India. Nd-Hf isotopic compositions of bedloads span a small range of values ( $-18 < \epsilon_{\text{Nd}} < -16$  and  $-30 < \epsilon_{\text{Hf}} < -23$ ) and lie next to the terrestrial array in a  $\epsilon_{\text{Hf}}$  vs.  $\epsilon_{\text{Nd}}$  diagram. Nd isotopic compositions are similar to those of the main Himalayan sources. By contrast, suspended loads have much more variable ratios ( $-19 < \epsilon_{\text{Nd}} < -10$  and  $-25 < \epsilon_{\text{Hf}} < -7$ ) and plot well above the terrestrial array in a  $\epsilon_{\text{Hf}}$  vs.  $\epsilon_{\text{Nd}}$  diagram. Like oceanic sediments, they are characterized by high  $\epsilon_{\text{Hf}}$  compared to their  $\epsilon_{\text{Nd}}$ . We explain this Nd-Hf decoupling by mineralogical sorting, a process that enriches bottom sediments in coarse and dense minerals, such as unradiogenic zircons, while the surface sediments are enriched in fine material with radiogenic Hf signatures.

Bedloads and suspended loads, collected at the same sampling site at different depths in the Narayani and Ganga Rivers, share similar  $\epsilon_{\text{Nd}}$ . However, differences of about 5  $\epsilon_{\text{Nd}}$  and 15  $\epsilon_{\text{Hf}}$  units are observed between bedload and surface samples in the Yamuna River. In this river, both Nd and Hf isotopic ratios decrease from surface to bottom. We believe that part of the Hf isotopic variability is due to mineralogical sorting but the rest of it, together with the entire Nd range, results from provenance effects. While material transported by the Narayani and Ganga Rivers mainly originates from the highly-resistant crystalline and metamorphic rocks of the Himalayan range, the material present in the Yamuna River partly comes from the more weatherable basaltic Deccan traps. We thus suggest that bedloads and suspended loads do not carry similar provenance information in the Yamuna River. Material produced by the erosion of basalts has highly-radiogenic Nd-Hf isotopic signatures and is preferentially transported in suspension near the river surface. In contrast, crystalline and metamorphic erosion products of the Himalayas have less radiogenic isotopic signatures and are preferentially transported near the river bottom.

Our results demonstrate that bedloads and suspended loads do not necessarily share similar sediment sources. In addition, we show that Hf isotopic compositions of bedloads are good proxies of sediment sources in the Himalayan range. This is not the case of the Hf isotopic compositions of suspended loads, which resemble worldwide oceanic sediments. This suggests that the puzzling decoupling of Nd and Hf isotopes in oceanic fine-grain sediments could have its origin in continental areas.

**Signature of hydrothermal alteration in ground-magnetic surveys at Yellowstone National Park**

*J. M. Glen*<sup>2</sup>; *C. Bouligand*<sup>1</sup>; *D. K. McPhee*<sup>2</sup>;

1. ISTERRE, Universite Grenoble 1, CNRS, Grenoble, France.

2. U.S. Geological Survey, Menlo Park, CA, United States.

**Body:** Yellowstone National Park (YNP) hosts a very large hydrothermal system with over 10,000 thermal features. Although hydrothermal alteration in YNP has been extensively studied with field observations, remote-sensing imagery, and core drilling, the volume and geometry of hydrothermal systems at depth remain poorly constrained. Magnetic surveys can help to investigate buried hydrothermal alteration as demonstrated by the high-resolution aeromagnetic survey of YNP (Finn and Morgan, *J. Volcanol. Geotherm. Res.*, 115, 207–231, 2002). Results of this survey show that magnetic lows extend over and beyond areas of hydrothermal activity. This suggests large volumes of buried demagnetized rocks due to hydrothermal alteration of the volcanic substratum. Although the interpretation of magnetic anomalies is non-unique, Finn and Morgan (2002) used these magnetic lows to estimate a minimum volume of buried altered rock assuming complete demagnetization of the substratum. This aeromagnetic survey was of relatively high resolution (flight line spacing < 500 m and flight elevation <350 m above ground), but it was insufficient for detailed mapping of individual thermal areas. In order to obtain a closer look at several areas, we performed ground-based magnetic surveys within YNP using a cesium-vapor magnetometer along 4-5 km long transects crossing four thermal areas (Norris Geyser Basin, Lower Geyser Basin, Lone Star Geyser Basin, and Smoke Jumper Hot-springs). We also performed a detailed survey over an area of about 800 m x 500 m around Lone Star Geyser. We also collected gravity data to help characterize the subsurface geologic structures and performed magnetic susceptibility, magnetic remanence, and density measurements on rock samples collected in the field and from drill cores collected in 1967-1968 to characterize physical properties of fresh and altered geologic units. The long magnetic transects show that magnetic anomalies are damped in altered areas suggesting a significant decrease in the magnetization of shallow volcanic units. The detailed magnetic map of the Lone Star Geyser displays a pronounced negative anomaly centered on the geyser mound and other hot-springs indicating demagnetization directly associated with the hydrothermal plumbing system. These surveys will be used to model the geometry of the demagnetized volcanic substratum associated with hydrothermal alteration.

**Lithospheric imaging from teleseismic data by frequency-domain elastic full-waveform tomography**

*D. Pageot*<sup>1</sup>; *S. Operto*<sup>1</sup>; *M. Vallée*<sup>1</sup>; *R. Brossier*<sup>2</sup>; *J. Virieux*<sup>2</sup>;

1. GeoAzur - Université Nice Sophia-Antipolis, Nice, France.
2. ISTerre - Université Joseph Fourier, Grenoble, France.

**Body:** The objective of this study is to adapt existing frequency-domain full-waveform tomographic (FWT) code, designed for controlled source experiments, for teleseismic body wave observations. Frequency-domain FWT seeks to estimate the elastic properties of the Earth by minimizing a misfit function between recorded and modeled full wavefields. FWT processed each frequency of a serie, independantly and successively, from the lower to the higher, and added contribution of each frequency to the model to build up progressively.

In the framework of teleseismic experiments, sources can be treated as planewaves impinging the base of the model and are characterized by incidence and obliquity angles. The full wavefield is computed using a scatterfield formulation in the frequency domain. First, a homogeneous background model and the corresponding analytical planewave solution are defined, then, a scattering source is formed by the product of the analytical planewave with the difference of the forward problem operators associated with the homogeneous background and lithospheric models. The scatter wavefield is then computed by performing a simulation in the lithospheric model using the scattering source. Finally, the full wavefield is built by summation of the analytical planewave and the scatter wavefields.

Compared to controlled source experiments, teleseismic experiments are characterized by a sparse source and station coverage which leads to a narrow illumination of aperture and a small amount of data. This requires the use of finely-sampled frequencies to prevent spatial aliasing in the reconstructed FWT models and to consider all reflections and conversions from the lithospheric reflectors generated after a first reflection from the free surface to overcome the limited resolution power of planewaves.

In the case of real experiments, teleseisms will propagate with an obliquity angle accross the lithospheric target defined by a 2D vertical plane below the stations. To take into account this obliquity angle, which correspond to back-azimuth, we apply an obliquity correction factor to velocity models to obtain apparent velocity models which allows to retrieve the correct wave propagation in the plane of the model.

The specific objective is to apply planewave FWT to real teleseismic dataset as, for example, Middle America Subduction Experiment which proposes to sample the Pacific subduction of Mexico to provide the subduction system geometry.

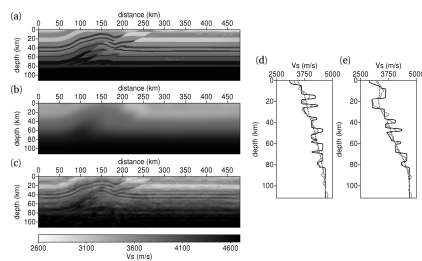


Figure 1: (a,b,c) S-wave velocity models corresponding to (a) True synthetic model,(b) initial synthetic model for inversion and (c) FWT model. Inversion was made for thirtion planewaves ranging from -40 to 40 degrees, 9 frequencies from 0.2Hz to 0.5Hz, 399 receivers with a step of 120km and 15 iterations per frequency. (d,e) Velocity logs at (d) 120km and (e) 350km, the solid black line correspond to (a), dot black line to (b) and gray solid line to (c).

Final ID: S41B-2192

**Seismic Surface-wave Tomography From Cross-correlations Of Ambient Noise At The Valhall Oil Field.**

*A. Mordret*<sup>1</sup>; *M. Landès*<sup>4</sup>; *N. M. Shapiro*<sup>1</sup>; *S. C. Singh*<sup>2</sup>; *P. Roux*<sup>3</sup>; *O. I. Barkved*<sup>5</sup>;

1. Seismology, IPGP, Paris, France.
2. Marine Geoscience, IPGP, Paris, France.
3. ISTERre, Grenoble, France.
4. CEA, Bruyères-le-Châtel, France.
5. BP, Stavanger, Norway.

**Body:** Here we present cross-correlation analysis of 6 hours of noise data recorded by a network of 3D multi-component ocean bottom cable at the Valhall Life of Field. The 2413 sensors were spaced at 50 m along 10 km long line and line spacing was 300 m. At 0.4- 2 Hz frequencies, the best signal-to-noise ratio was obtained for vertical-vertical (VV) cross-correlations that clearly show Scholte waves. At higher frequencies (3–30 Hz), the seismic noise is mainly produced by the exploitation platform at the center of the network and the highest signal-to-noise ratio was obtained on transverse-transverse (TT) cross-correlations, which was dominated by Love's waves. Because of the localized noise source at these high frequencies, we selected a profile of stations suitably aligned relative to the platform and computed TT cross-correlations between all pairs of stations. We then extracted dispersion curves and inverted them to construct a 2D shear-velocity profile down to 20 m depth. We find that upper strata of the sediments have velocities of 200- 400 m/s and vary laterally, which is extremely important for S-wave statics. At low frequencies, we computed VV cross-correlations for all possible station pairs. We then measured Scholte wave group velocity dispersion curves and inverted them to build group velocity maps of the Valhall area. Similar to previously published models from full waveform inversion of an active seismic dataset, our results show a coherent pattern dominated by paleo-channels at the seabed above the Valhall field. Our results show that a detailed 3D S-wave velocity could be determined using noise data collected by permanent ocean bottom cables.

## MINERALOGICAL AND GEOCHEMICAL EVOLUTION OF ALPINE SERPENTINITES DURING SUBDUCTION DYNAMICS

*S. Schwartz*<sup>1</sup>; *R. Lafay*<sup>1</sup>; *F. Deschamps*<sup>2</sup>; *S. Guillot*<sup>1</sup>; *C. Nicollet*<sup>3</sup>;

1. IsTerre, Grenoble University - CNRS, Grenoble, France.

2. Geosciences Montpellier, Montpellier University - CNRS, Montpellier, France.

3. Laboratoire Magmas et Volcans, Blaise Pascal University - CNRS, Clermont-Ferrand, France.

**Body:** Serpentinites observed in accretionary wedge of the western Alps result from two serpentinization processes: (i) during fluid/rock interactions in oceanic context and (ii) during the first step of subduction. Progressive serpentinization from the ridge to subduction zone affects physical, geochemical and rheological properties of the oceanic lithosphere. Exhumed serpentinite units are commonly characterized by different co-stability serpentine species (chrysotile, lizardite and antigorite).

Field stability of these three serpentine species remains poorly constrained. To understand and clarify their respective stability domain in subduction context, we studied alpine serpentinites under different high pressure conditions. In this paleo-accretionary wedge, different oceanic units have been metamorphosed from low temperature blueschist facies conditions ( $T < 350$ ;  $P < 1$  GPa) to eclogitic facies conditions ( $T > 500$ °C,  $P > 2$  GPa).

Based on Raman spectroscopy analysis, we estimate the metamorphic temperature conditions reached by selected samples and we characterize the serpentine species associations. Our results show a progressive destabilization of lizardite/chrysotile in favor of antigorite along the increasing subduction gradient.

Additionally, our geochemical bulk rocks and in situ (LA-HR-ICP-MS) analysis on serpentinites and associated metasediments indicates a progressive enrichment in fluid-mobile elements (FME: As, B, Li, Sb) during increasing of metamorphic conditions. This highlights elementary exchange and fluids circulation between metasediments and serpentinites into the accretionary wedge. We propose that FME from metasediments are transferred by water and silica rich fluids at mantle depths into serpentinites which constitute a secondary reservoir for these elements.

Final ID: V41C-2513

### Origin of multiple serpentinization events in New Caledonia

*M. Ulrich*<sup>1</sup>; *S. Guillot*<sup>1</sup>; *M. Muñoz*<sup>1</sup>; *C. Picard*<sup>2</sup>;

1. ISTERre, University of Grenoble, Grenoble Cedex 9, France.

2. Chrono-environnement, University of Franche-Comté, Besançon, France.

**Body:** Studies on serpentinites around the world have shown that various polymorphs can coexist depending on the temperature, pressure and chemistry of the formation environment. Identifying serpentine polymorphs can thus provide significant constraints on the geodynamic environment at the time of formation. The New Caledonia ophiolite (Southwest Pacific) is one of the world's largest (500 km long, 50 km wide and 2 km thick). Emplaced during Eocene, it is thrust upon the continental Norfolk ridge, which derived from the splitting of the East Gondwana margin during Lower Late Cretaceous. The ophiolite consists of a large continuous massif occurring in the south of the island and some smaller isolated klippen located along the West coast. The peridotites are mostly harzburgite, related to a supra-subduction zone environment. The northernmost massifs are also composed of lherzolites, inherited from the opening of the South Loyalty Basin where the ophiolite was formed. Serpentinization is ubiquitous (usually >50%) independently from the nature of the peridotite. However, numerous studies have focused on the ophiolite but very few on the serpentinite. In this study, we use the Raman spectroscopy to identify serpentine polymorph in each part of the ophiolite. In situ trace element measurements were performed to constrain the behavior of fluid mobile element (FME: As, Sb, B, Li, Cs, Pb, U, Ba, Sr), and we are currently analyzing stable isotopic ratios to investigate the origin of fluids. Our results show that lizardite represents ~90% of the serpentine in the New Caledonia ophiolite. Only the serpentinite has recorded multiple serpentinization events. In this horizon, the lizardite is crosscut by millimeter to centimeter antigorite veins. Chrysotile is the last polymorph to crystallize in millimeter crackseals. If the formation of the lizardite can be easily related to abyssal history of the ophiolite for the lherzolite and its supra-subduction history for the harzburgite, the origin of the antigorite veins is more questionable. P-T conditions required to form this polymorph together with FME enrichments indicate that the antigorite veins could derive from the circulation of metasomatic fluids related to the isothermal exhumation of HP rocks (i.e. the Diahot terrane) responsible for the heat advection beneath the ophiolite. Oxygen isotopes indicate that chrysotile was formed later (likely during the obduction) by the circulation of meteoric fluids.

**Dehydration reactions, mass transfer and rock deformation relationships during subduction of Alpine metabauxites: insights from LIBS compositional profiles between metamorphic veins**

*A. Verlaquet*<sup>1</sup>; *F. Brunet*<sup>2</sup>; *B. Goffe*<sup>3</sup>; *D. Menut*<sup>4</sup>; *N. Findling*<sup>2</sup>; *C. Poinssot*<sup>5</sup>;

1. IStEP, Univ Paris 6 - UPMC, Paris, France.
2. ISterre, Univ Grenoble 1, Grenoble, France.
3. CEREGE, Aix-en-Provence, France.
4. DEN, CEA Saclay, Gif-sur-Yvette, France.
5. DEN, CEA Marcoule, Bagnols-sur-Cèze, France.

**Body:** In subduction zones, the significant amounts of aqueous fluid released in the course of the successive dehydration reactions occurring during prograde metamorphism are expected to strongly influence the rock rheology, as well as kinetics of metamorphic reactions and mass transfer efficiency. Mineralized veins, ubiquitous in metamorphic rocks, can be seen as preserved witnesses of fluid and mass redistribution that partly accommodate the rock deformation (lateral segregation). However, the driving forces and mechanisms of mass transfer towards fluid-filled open spaces remain somewhat unclear. The aim of this study is to investigate the modalities of mass transfer during local fluid-rock interactions, and their links with fluid production and rock deformation.

This study focuses on karstic pockets (metre scale) of Triassic metabauxites embedded in thick carbonate units, that have been isolated from large-scale fluid flow during HP-LT Alpine metamorphism (W. Vanoise, French Alps). These rocks display several generations of metamorphic veins containing various Al-bearing minerals, which give particular insights into mass transfer processes.

It is proposed that the internally-derived fluid (~13 vol% produced by successive dehydration reactions) has promoted the opening of fluid-filled open spaces (euhedral habits of vein minerals) and served as medium for diffusive mass transfer from rock to vein. Based on mineralogical and textural features, two vein types can be distinguished: (1) some veins are filled with newly formed products of either prograde (chloritoid) or retrograde (chlorite) metamorphic reactions; in this case, fluid-filled open spaces seem to offer energetically favourable nucleation/growth sites; (2) the second vein type is filled with cookeite (Li-Al-rich chlorite) or pyrophyllite, that were present in the host rock prior to the vein formation. In this closed chemical system, mass transfer from rock to vein was achieved through the fluid, in a dissolution-transport-precipitation process, possibly stress-assisted.

Cookeite is highly concentrated (40-70 vol%) in regularly spaced veins. Laser Induced Breakdown Spectroscopy profiles show that cookeite is evenly distributed in the rock matrix comprised between two veins. The absence of diffusion profiles suggests that the characteristic diffusion length for Li, Al and Si is greater than or equal to the distance separating two cookeite veins (3-6 cm). This is in agreement with characteristic diffusion lengths calculated from both grain boundary and pore fluid diffusion coefficients, for the estimated duration of the peak of metamorphism. Phyllosilicates have very different morphologies in the rock matrix (fibers) compared to veins (euhedral crystals): fluid-mineral interfacial energy may be maximal in the small matrix pores, which can maintain higher cookeite solubility than in fluid-filled open spaces. Therefore, as soon as veins open, chemical potential gradients may develop and drive cookeite transfer from rock matrix to veins.

Final ID: T41B-07

## Development of roughness in pressure solution interfaces and consequence for the ductile rheology of the upper crust

*(Invited)*

*F. Renard*<sup>1, 2</sup>; *J. Gratier*<sup>1</sup>; *D. K. Dysthe*<sup>2</sup>;

1. ISTERre, Université Joseph Fourier, Grenoble, France.

2. PGP, University of Oslo, Oslo, Norway.

**Body:** Field observations indicate that ductile deformations are present in the Earth's upper crust, such as folding, fault creep, earthquake afterslip, slow earthquakes, or slow displacements of landslides, as well as compaction of sedimentary rocks or fault gouge. Several experimental studies have analyzed various mechanisms responsible for this slow creep. One of these mechanisms is pressure solution creep, a ductile process activated by the presence of reactive fluids and enhanced by local stress gradients that promote dissolution and reprecipitation of soluble rocks. Laboratory experiments and theory have shown that the time dependence of pressure solution creep can be variable, the strain being either linear in time (i.e. viscous flow), or with logarithmic or power law time dependence, making difficult to build rheological models.

Here, we present experimental results of pressure solution creep of either single crystal indentation or aggregate compaction of quartz, calcite, and halite, three major soluble minerals in the upper crust. We monitor the time evolution of the deformation and characterize its non-linear time dependence that usually follows a power law with a small time exponent, in the range 0.2-0.4. A quite large variability of the strain rate in experiments under equivalent conditions is also observed. In addition, we measured the topography (i.e. roughness) of several mineral interfaces under stress after each experiment and observed that this micro-roughness shows also power-law dependence in space. Interestingly, the pressure solution strain rate is correlated with the amplitude of the roughness at the end of the experiments: the rougher the surface, the faster the deformation. Using micro-acoustic sensors that allow recording the elastic waves emitted during frictional sliding on reactive rough interfaces, we show that roughness amplitude variations could also be related to the emission of tremor-like seismic signals, correlated to the presence of slow slip events at the laboratory scale.

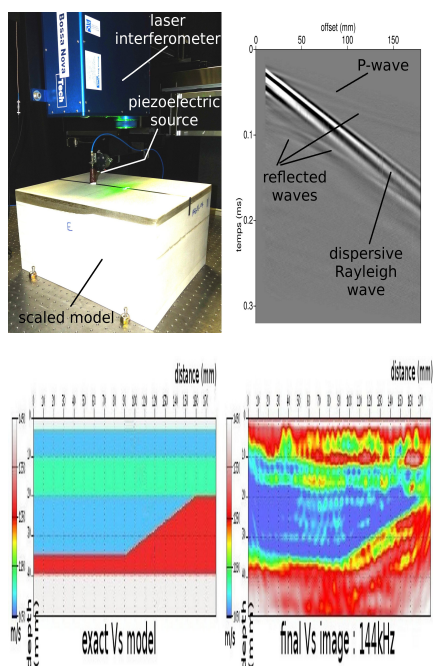
Roughness of interfaces under stress seems therefore to represent a key parameter that controls the overall rate of deformation. Initial roughness is controlled by the processes at the origin of the interface such as sedimentation in basins or damage in fault zones. It then evolves in time and modifies the overall rate of deformation. Experiments show that this roughness evolves because of the presence of heterogeneities in the rock and the driving effect of local stress. Theoretical considerations and numerical simulations also show that a flat interface under stress should become rough because the rough state minimizes the total energy compared to the flat interface case. This roughness follows non-linear time dependence that represents a balance between stabilizing and destabilizing processes and the existence of equilibrium or a steady state roughness is still debated. The existence of dynamic equilibrium of interface roughness could account for memory effects during ductile deformation of the rocks in the upper crust.

**Small scale seismic measurement bench to assess imaging methods – application to Full Waveform Inversion of a shallow structure.**

*F. Bretaudeau*<sup>2, 1</sup>; *D. Leparoux*<sup>1</sup>; *R. Brossier*<sup>3</sup>; *S. Operto*<sup>4</sup>; *J. Virieux*<sup>3</sup>;

1. MACS, IFSTTAR, Bouguenais, France.
2. DEI / SARG / BERSSIN, IRSN, Fontenay-aux-Roses, France.
3. ISTERRE, Grenoble, France.
4. GeoAzur, Nice, France.

**Body:** Seismic imaging of subsurface is useful for civil engineering and landscape management topics. The usual methods use surface waves phase velocities or first arrival times of body waves. However, for complex structures, such methods can be inefficient and Full Waveform Inversion (FWI) promises relevant performances because all the signal is taken into account. FWI has been originally developed for deep explorations (Pratt et al. 1999). Heterogeneities and strong attenuation in the near surface make difficult the adaptation of the FWI to shallower media (Bretaudeau et al. 2009). For this reason, we have developed a physical modeling measurement bench that performs small scale seismic recording in well controlled contexts (Bretaudeau et al. 2011). In this paper we assess the capacity of the FWI method (Brossier 2010) for imaging a subsurface structure including a low velocity layer and a lateral variation of interfaces. The analog model is a 180mm long and 50mm thick layered epoxy resin block (fig. 1). Seismic data generated with a punctual piezoelectric source emitting a 120KHz Ricker wavelet at the medium surface were collected by an heterodyne laser interferometer. The laser allows recording the absolute normal particle displacement without contact, avoiding disturbances caused by coupling. The laser interferometer and the piezoelectric source were attached to automated arms that could be moved over the model surface to a precision of 0.01mm (fig. 1). The acquisition survey includes 241 receiver and 37 source positions respectively spaced at 1 and 5 mm. Figure 2 shows 2D maps of the Vs parameter after inversion of data sequentially processed with 13 frequencies. The geometry of the sloped interface is recovered. A low velocity zone is imaged but with a thickness thinner than expected. Moreover, artifacts appear in the near surface. Experimental modeling results showed the capacity of the FWI in this case and provided key issues for further works about inversion by FWI for subsurface topics.



Final ID: NG42A-03

**A dynamo driven by zonal jets at the upper surface: applications to giant planets (*Invited*)**

C. Guervilly,<sup>1, 2</sup>; P. CARDIN;<sup>2</sup>; N. Schaeffer;<sup>2</sup>;

1. Applied Mathematics and Statistics, University of California Santa Cruz, Santa Cruz, CA, United States.

2. Institut des Sciences de la Terre, Université Joseph Fourier, CNRS, Grenoble, France.

**Body:** We present a dynamo mechanism arising from the presence of barotropically unstable zonal jet currents in a spherical shell. The shear instability of the zonal flow develops in the form of a global Rossby mode, whose azimuthal wavenumber depends on the width of the zonal jets. We obtain self-sustained magnetic fields at magnetic Reynolds numbers greater than 1,000. We show that the propagation of the Rossby waves is crucial for dynamo action. The amplitude of the axisymmetric poloidal magnetic field depends on the wavenumber of the Rossby mode, and then on the width of the zonal jets. We discuss the plausibility of this dynamo mechanism for generating the magnetic field of the giant planets. Our results suggest a possible link between the topology of the magnetic field and the profile of the zonal winds observed at the surface of the giant planets.

**Rheological Evolution of Faults During the Seismic Cycle: the Role of Pressure Solution Creep and Sealing Processes**

*J. Gratier*<sup>1</sup>; *F. Renard*<sup>1, 2</sup>; *J. Richard*<sup>1</sup>; *M. Doan*<sup>1</sup>; *B. Vial*<sup>1</sup>;

1. ISTERRE, Observatoire, Université Joseph Fourier, CNRS, Grenoble, France.

2. Physics of Geological Processes, University of Oslo, Oslo, Norway.

**Body:** Active faults in the upper crust can either slide steadily by aseismic creep, or abruptly causing earthquakes.

However, seismic and aseismic processes are often closely related: i.e. earthquakes are often followed by afterslip creep. In this case, postseismic displacement rates progressively decrease with time after several months, years or decades, and may reach an equivalent geodetic moment greater than the seismic moment released by the earthquake itself. In parallel, evidence of coseismic rock damage and postseismic healing of the same fault zone are recorded. So, at least at regional scale, postseismic healing rate and displacement rate seems to slow down similarly with time. Several questions arise from such observations: how seismic fracturing could trigger, or accelerate, afterslip creep? and why this effect progressively slows down with time? Conjugate studies of naturally deformed zone at depth and experimental deformation bring some answers.

Microstructural studies of samples collected from the San Andreas Fault Observatory at Depth (SAFOD) show that pressure solution creep, a stress driven mass transfer process, accommodates at least part of the aseismic creep of the San Andreas Fault. Mass transfer occurs from solution cleavage to fracture. Moreover, the creep rate was accelerated by the last M6 Parkfield event. Consequently pressure solution is clearly associated with fracturing process.

Here, we present pressure solution indenter experiments that show how grain-scale fracturing induced by dynamic stress loading drastically accelerates the displacement rate accommodated by pressure solution creep: fracturing opens new paths for solute transport along fluid-filled fractures, which decreases the distance of diffusion. However, as the fractures progressively seal, this effect disappears as sealing increases the distance of mass transfer and, consequently, reduces the displacement rate. We investigate the time-dependent evolution of indenter displacement after dynamic stress loading (i.e. ball drop on the indenter) and compare it with postseismic non-linear displacement in nature. Experimental displacement/time relations can most often be fitted by power laws with some variations in the power exponents that depend on the roughness of the dissolution surface, the nature of the minerals, the texture and initial porosity of the rocks.

In conclusion, both observation of natural deformation and experimental results show the crucial role of pressure solution creep and sealing processes in the dynamic interaction of pressure solution and fracturing: fracturing associated with earthquakes activates pressure solution creep rate by reducing the distance of mass transfer; and dissolution increases soluble species content in the fluid facilitating the progressive healing of the coseismic fracture network and strengthening the fault.

Final ID: S43B-2229

**Determination of the source time function of seismic event by blind deconvolution of regional coda wavefield: application to December 22, 2009 explosion at Kambarata, Kyrgyzstan**

*O. G. Sebe*<sup>1</sup>; *J. Guilbert*<sup>1</sup>; *P. Bard*<sup>2</sup>;

1. CEA, DAM, DIF, F-91297, ARPAJON, France.

2. Institut des Sciences de la Terre, Université Joseph Fourier, F-38041 Grenoble, France.

**Body:** At regional distance, recovering the source time function of a seismic event is a rather difficult task as the Green function is unknown due to large scattering of the waves by crust heterogeneities. Contrary to classical methods based on deterministic assessment of the Green function, this work proposes to exploit the stochastic nature of regional coda wavefield in order to extract the seismic source time function of a regional event.

Since the work of Aki and Chouet 1975, it is well recognized that regional coda waves can provide stable and robust information on the source of seismic events. Unfortunately, all the proposed techniques are limited to the power spectral density of the seismic source function.

A modified version of our two step spectral factorization algorithm [Sèbe et al. 2005] of coda waves has been proposed in order to include higher order statistic (HOS) blind deconvolution techniques. Assuming that the coda excitation time series is a non-Gaussian independent and identically distributed random signal, the higher order statistics, especially the tricorrelation, is able to remove the randomness of coda excitation and extract source properties. In addition, unlike classical second order approach which only provides the power spectral density, the tricorrelation keeps the information on the phase spectrum of the source, allowing the estimation of the source time function.

This original blind deconvolution algorithm of coda waves has been applied on the regional records of the December 22, 2009 explosion in Kambara, Kyrgyzstan. Based on statistic analyses of the higher order cumulants, this method has been able to recover the main properties of the source time function of this detonation: two successive explosions have been identified with a time delay of about 1.7 sec and an amplitude ratio of about 2 in favour of second explosion. This successful blind recovering of high resolution source properties is an encouraging result toward the development of new source characterization methods especially when the classical deconvolution techniques are unusable due to the Green's function complexity or unknown.

Final ID: S43B-2235

### Using teleseismic data to improve the depth estimation of the 07th of July 2011 Corsica event

*J. Letort*<sup>1,2</sup>; *J. Guilbert*<sup>2</sup>; *J. Vergoz*<sup>2</sup>; *Y. Cano*<sup>2</sup>; *O. G. Sebe*<sup>2</sup>; *F. Cotton*<sup>1</sup>;

1. ISTERRE, Grenoble, France.

2. CEA, DASE/LDG, Bruyere le Chatel, France.

**Body:** The 07th of July 2011 at 07:21pm a moderate earthquake ( $m_b=5.3$  according to LDG/CEA), 100km west from Ajaccio, shacked Corsica and coastal areas in south of France. This earthquake has been the strongest since nearly 40 years in this densely populated area. The focal mechanism determination shows that the event occurred on an inverse fault NE-SW oriented. This style of faulting is very well constrained by waveform inversion, using regional dataset (GEO- AZUR Nice, INGV Rome) as well as teleseismic data (LDG/CEA). The epicenter is localised in a transition zone between the Corsican continental crust and a complex narrow oceanic-type basement, the Ligurian Sea.

However, surprisingly enough, the depth estimation gives different results when working with surface waves at regional distances (depth around 10km) and when using depth phases recognition methods at teleseismic distance (25km deep). The minimisation of the regional arrival times residuals and the empirical fact that the event has been felt far enough tend to confirm a deeper hypocentral depth. At regional scales, the resolution is limited given the narrow azimuthal coverage (stations mainly in mainland France). Moreover, the depth indetermination might be caused by the sensitivity of surface wave propagation to the heterogeneities into the crust, which are particularly high in this area.

Based on LDG and IDC teleseismic dataset, coherent depth phases have been detected using cepstral based methods and genetic algorithm inversions. All these methods confirm a deeper hypocenter than found by previous regional inversion. Different crust models have been tested and depth phases have been then analysed as possible pP, wP or sP waves to assess the influence of the phase type on depth estimation. In this particular study case, teleseismic data constrain more efficiently the hypocentral depth.

More generally, for superficial and noisy earthquakes, regional estimation seems appropriated and for deeper and in complex crustal area earthquakes, we should use teleseismic data to improve the depth resolution, as seen for this event.

Hence, using arrays to lower the signal to noise ratio and with recent data quality improvements, the teleseismic approach seems an interesting way for quasi-automated depth estimation of moderate earthquakes. Depth estimation is a burning issue for the Comprehensive-Test-Ban-Treaty Organization (CTBTO), as a constrained depth is a means to discriminate between explosions (shallow) and earthquakes. It is also well known, but not yet fully proved, that focal depths play a role on macroseismic intensities and ground motion amplitudes.

Teleseismic depth estimation, would be now widely used and tested for CTBTO monitoring objectives as well as to study depth influence on earthquakes properties.

Final ID: V43E-08

**The Lesser Antilles: a case study for melt-dehydration processes in arcs**

*C. Chauvel*<sup>1</sup>; *S. Labanieh*<sup>1</sup>; *M. Carpentier*<sup>1, 2</sup>;

1. ISTERre, Grenoble, France.

2. Univ British Columbia, Vancouver, BC, Canada.

**Body:** The nature and the proportion of subducted material involved in the genesis of island arcs depends on the amount and type of subducted sediments, the input from basaltic crust, the mechanism of chemical transfer and the speed and angle of the subducting plate.

Here we present a compilation of geochemical features along the Lesser Antilles arc which is famous for having the most “continental crust-like” geochemical characteristics of all island arcs. We show that beneath the southern part of the Lesser Antilles arc, where vast amounts of sedimentary material are subducted, sediments melt to produce island arc magmas with elevated La/Yb and low Ba/Th, U/Th, Sr/Th and Pb/Th. Associated with these trace element characteristics are typically crustal isotopic signatures: low  $^{143}\text{Nd}/^{144}\text{Nd}$  and  $^{176}\text{Hf}/^{177}\text{Hf}$  and high  $^{87}\text{Sr}/^{86}\text{Sr}$  and Pb isotopic ratios. In contrast, in the northern part of the arc, where far less sediment enters the trench, La/Yb is low and associated to high Ba/Th, U/Th, Sr/Th and Pb/Th in all lavas, and radiogenic isotope ratios are near those of MORB. In this part of the island arc, dehydration of altered basalt is responsible for the enrichment in fluid-mobile elements (Ba, U, Sr, Pb etc..) and the subducted sediments are barely involved. On Martinique in the middle of the arc, both types of lavas exist but not in the same place. On the west side of the island, sediment melting dominates while dehydration of basalt controls the volcanism closer to the trench.

This dichotomy between sediment melting and slab dehydration appears a worldwide feature: in Sunda, Luzon and Banda arcs, subducted sediment melts to produce lavas with high La/Yb, low Ba/Th, U/Th, Sr/Th and Pb/Th and “crust-like” radiogenic isotopic characteristics. In contrast, in Izu-Bonin-Mariana, Tonga and Kermadec arcs, fluid migration leading to high mobile/immobile trace element ratios and “mantle-like” isotopes controls element transport from the subducted slab. The only arcs similar to the Lesser Antilles, where both processes occur at different times or in different locations, are the Scotia, Kurile, Bismark and Aleutian arcs.

While the enriched isotopic signature due to sediment melting is fairly simple to understand, this is not the case for the depleted end member of all arcs. In all arcs, particularly the fluid-dominated ones where Sr/Th can reach several thousand,  $^{87}\text{Sr}/^{86}\text{Sr}$  is buffered at a value around 0.7030 - 0.7035 suggesting that the Sr in fluids comes not from the sedimentary pile but from the subducted basaltic crust. Given the difficulty in conceiving that fluids can travel through a large section of sedimentary material without interacting with it, this observation implies that the sedimentary cover is often inexistent where magma forms.

Final ID: V44B-06

**Scientific Drilling in the Barberton Greenstone Belt, South Africa**

N. Arndt<sup>1</sup>;

1. ISTERre, University of Grenoble, Grenoble, France.

**Body:** The Barberton Greenstone Belt in South Africa, one of the best-preserved successions of mid-Archean (3.5-3.2 Ga) supracrustal rocks in the world, is a remarkable natural laboratory where conditions and processes at the surface of the Archean Earth can be studied in detail. Despite generally good outcrop, complete field sections are not preserved, and crucial features such as the contacts of lava flows and continuous successions of critical sedimentary rock sequences are not exposed. Through diamond drilling we hope to obtain the continuous sections and relatively unaltered samples through the volcano-sedimentary successions. (1) Sedimentary sequences will provide information about erosion and sedimentation on the early Earth, the composition and temperature of Archean seawater, and one possible site where life may have emerged and evolved. Investigation of spherule layers (including impact debris) will provide information about the nature and magnitude of meteorite impact on the early Earth. (2) Successions of ultramafic to mafic volcanic rocks will provide new insights into volcanic processes, dynamics of the crust and mantle, interaction between oceanic volcanic crust and the hydrosphere and biosphere. The sources of hydrothermal fluids on the ocean floor, driven by circulation of seawater through the volcanic pile, constitute a second habitat of early life.

A project supported by the International Continental Drilling Program and by scientists from 13 countries in five continents started on 15th July 2011. As of 31st July, two holes have been drilled in komatiites from the Tjakastad locality and another hole has been started in the Buck Reef Chert. Regular updates are available on the ICDP web site < [www.icdp-online.org](http://www.icdp-online.org)>. The distribution of samples and post-drilling research will be coordinated by a steering committee comprising representatives from all major participating countries. A workshop to decide who does what will be held in South Africa in early 2012 and core will then be distributed to interested scientists.

Final ID: H51G-1262

## From Nm-Scale Measurements Of Mineral Dissolution Rate To Overall Dissolution Rate Laws: A Case Study Based On Diopside

*D. Daval*<sup>1</sup>; *G. Saldi*<sup>1</sup>; *R. Hellmann*<sup>2</sup>; *K. Knauss*<sup>1</sup>;

1. Earth Sciences Division, Lawrence Berkeley National Lab, Berkeley, CA, United States.

2. ISTerre, CNRS/UJF, Grenoble, France.

**Body:** While we expect conventional reactive transport simulations to provide reliable estimations of the evolution of fluid-rock interactions over time scales of centuries and even more, recent experimental studies showed that they could hardly be satisfactorily used on simplified systems (e.g. batch carbonation experiments on single minerals), on time scales of weeks [1]. Among the reasons for such inconsistencies is the nature of the rate laws used in the geochemical codes, which heavily relies on our description of the fundamental mechanisms involved during water(-CO<sub>2</sub>)-mineral reactions.

Silicate dissolution constitutes a key step of GCS processes. Whereas the dissolution rate of silicate minerals has been extensively studied at far-from-equilibrium conditions, extrapolating such rates over a broad range of solution composition relevant for GCS has proven challenging. Regarding diopside, recent studies [2, 3] suggested that below 125 °C, an unexpected drop of the rate occurred for Gibbs free energies of reaction ( $\Delta Gr$ ) as low as  $-76 \text{ kJ.mol}^{-1}$ , with severe consequences on our ability to predict the rate of complex processes such as carbonation reactions [3].

The mechanism responsible for such a drop remains unclear and therefore needs to be deciphered. An examination of our previous data [3] led us to envisage that two different, non-exclusive aspects were worth investigating: (i) the possible passivating ability of interfacial, nm-thick Si-rich layers developed on weathered silicate surface, and (ii) the stop of etch pits formation on crystal surface, each mechanism being found to be responsible for drops of olivine [1] and albite [4] dissolution rates, respectively.

Our ongoing experiments aim at better constraining these two mechanisms, and determining in turn whether one of them could explain the above-mentioned drop of diopside dissolution rate. Classical flow-through experiments with controlled SiO<sub>2</sub>(aq) concentrations are combined with both ex situ AFM and VSI measurements and in situ monitoring of the topography of the dissolving surface of diopside in a hydrothermal AFM flow-cell (e.g. [5]). By investigating the dissolution of several cleavages, we will show how these latter techniques represent a powerful tool for studying the anisotropy of diopside dissolution, and determining which face ultimately controls its dissolution rate. An attempt to link these observations to macroscopic determination of diopside dissolution rates as a function of fluid composition will be discussed.

[1] Daval et al. (2011) *Chem. Geol.*, 284, 193-209.

[2] Dixit & Carroll (2007) *Geochem. T.*, 8, 1-14.

[3] Daval et al. (2010) *Geochim. Cosmochim. Ac.*, 74, 2615-2633.

[4] Arvidson & Luttge (2010) *Chem. Geol.*, 269, 79-88.

[5] Saldi et al. (2009) *Geochim. Cosmochim. Ac.*, 73, 5646-5657.

Final ID: NG51D-1673

## Damage dynamics inferred from acoustic emissions in a partially frozen rock-wall

*L. Girard*<sup>1</sup>; *S. Gruber*<sup>1</sup>; *D. Amitrano*<sup>2</sup>;

1. 3G, Dep. of Geography, University of Zurich, Zurich, Switzerland.

2. ISTerre, CNRS - Université Joseph Fourier Grenoble, Grenoble, France.

**Body:** The formation of ice within rock is an important driver of rock damage near the surface and up to several meters depth. In steep terrain, this process may be crucial for the slow preconditioning of rock fall from warming permafrost areas.

Laboratory experiments as well as theoretical studies have contributed to clarify the basic mechanisms through which ice formation can damage rock: (i) the difference in density between the liquid water and the ice crystal, which results in the initial build-up of an in-pore pressure at the onset of crystallization and (ii) the cryo-suction process, which drives liquid water towards already frozen pores as the temperature further decreases.

However, the transfer of corresponding theoretical insight and laboratory evidence to natural conditions characterized by strong spatial and temporal heterogeneity is nontrivial. To prepare corresponding characterization of rock damage in natural conditions, we monitored the acoustic emission (AE) activity induced by natural thermal cycling and freeze/thaw in a rock-wall located in the Swiss Alps at 3500m a.s.l., in April 2010.

During the measurements period the rock temperature at the surface underwent large diurnal temperature cycles through 0°C, while it remained continuously below 0°C at depth greater than about 20 cm. A wealth of AE events was recorded on all 6 sensors deployed. Large bursts of activity are shown to occur during freezing periods, in locations that are provided with liquid water during diurnal melt. A robust power-law distribution of AE event energy and time is reported for all sensors. This common observation of the dynamics of rupture processes is a strong indication of freezing-induced damage.

The b-value of the probability distribution function of AE event energy is 1.6 for all sensors. This value is in the range expected for rocks and is very close to that obtained in laboratory experiments prior to the peak load or for creep of compression tests after the onset of tertiary creep, as well as for seismic forerunners recorded in a cliff before its collapse. In our case the loading mode is very different, since it results from local in-pore pressure variations.

We are currently working on the deployment of a continuous monitoring installation that will allow us to improve our understanding of freezing induced damage by estimating the depth of AE sources, the rock temperature and liquid water content variations.

Final ID: NS51B-1746

**Modeling and inversion Matlab algorithms for resistivity, induced polarization and seismic data.**

*M. Karaoulis*<sup>1</sup>; *A. Revil*<sup>1, 4</sup>; *B. J. Minsley*<sup>3</sup>; *D. D. Werkema*<sup>2</sup>;

1. Colorado School of Mines, Golden, CO, United States.

2. U.S. EPA, Las Vegas, NV, United States.

3. USGS, Lakewood, CO, United States.

4. ISTERre CNRS, Le Bourget du Lac, France.

**Body:** M. Karaoulis (1), D.D. Werkema (3), A. Revil (1,2), A., , B. Minsley (4),

(1) Colorado School of Mines, Dept. of Geophysics, Golden, CO, USA.

(2) ISTERre, CNRS, UMR 5559, Université de Savoie, Equipe Volcan, Le Bourget du Lac, France.

(3) U.S. EPA, ORD, NERL, ESD, CMB, Las Vegas, Nevada, USA .

(4) USGS, Federal Center, Lakewood, 10, 80225-0046, CO.

**Abstract**

We propose 2D and 3D forward modeling and inversion package for DC resistivity, time domain induced polarization (IP), frequency-domain IP, and seismic refraction data. For the resistivity and IP case, discretization is based on rectangular cells, where each cell has an unknown resistivity in the case of DC modelling, resistivity and chargeability in the time domain IP modelling, and complex resistivity in the spectral IP modelling. The governing partial-differential equations are solved with the finite element method, which can be applied to both real and complex variables that are solved for. For the seismic case, forward modeling is based on solving the eikonal equation using a second-order fast marching method. The wavepaths are materialized by Fresnel volumes rather than by conventional rays. This approach accounts for complicated velocity models and is advantageous because it considers frequency effects on the velocity resolution. The inversion can accommodate data at a single time step, or as a time-lapse dataset if the geophysical data are gathered for monitoring purposes. The aim of time-lapse inversion is to find the change in the velocities or resistivities of each model cell as a function of time. Different time-lapse algorithms can be applied such as independent inversion, difference inversion, 4D inversion, and 4D active time constraint inversion. The forward algorithms are benchmarked against analytical solutions and inversion results are compared with existing ones. The algorithms are packaged as Matlab codes with a simple Graphical User Interface. Although the code is parallelized for multi-core cpus, it is not as fast as machine code. In the case of large datasets, someone should consider transferring parts of the code to C or Fortran through mex files. This code is available through EPA's website on the following link <http://www.epa.gov/esd/cmb/GeophysicsWebsite/index.html>

Although this work was reviewed by EPA and approved for publication, it may not necessarily reflect official Agency policy.

Final ID: DI51B-2139

**Seismic anisotropy of the inner core deduced from geodynamical and mineralogical models**

*P. CARDIN*<sup>1</sup>; *A. Lincot*<sup>1</sup>; *S. Merkel*<sup>2</sup>; *R. Deguen*<sup>3</sup>;

1. ISTerre, Université Grenoble 1/CNRS, Grenoble, France.
2. UMET, Université Lille1/CNRS, Lille, France.
3. EPS, Johns Hopkins University, Baltimore, MD, United States.

**Body:** We generate different geodynamical models of formation of the inner core which take into account differential growth, stratification, thermal convection, magnetic forces. According to the relative importance of the different processes, the time evolution and the present day inner core show a large variability. Then, we use a visco plastic standard model to compute the lattice preferred orientation generated during the geodynamical deformation process. Using the elastic constants of different solid phase of iron at the inner core conditions, we compute the variation (amplitude and direction) of the P-wave velocity in the inner core. Then, we represent these results as maps/graph of travelling time anomalies which can be easily compared to real seismological data. These comparisons lead us to propose a preferred model of the growth evolution of the inner core.

**Uncertainty of permeability and specific storage due to experimental error during data acquisition for pulse-transient technique**

*I. Song*<sup>1, 3</sup>; *A. P. Rathbun*<sup>2, 3</sup>; *D. M. Saffer*<sup>3</sup>;

1. Division of Geologic Environment, Korea Inst. Geosc. & Min. Res., Daejeon, Korea, Republic of.

2. ISTerre, University Joseph Fourier – Grenoble I & CNRS, Grenoble, France.

3. Department of Geosciences and Center for Geomechanics, Geofluids, and Geohazards, The Pennsylvania State University, University Park, PA, United States.

**Body:** Transient fluid flow through rock is governed by two hydraulic properties: permeability ( $k$ ) and the specific storage ( $S_s$ ), which are often determined by the pulse-transient technique when  $k$  is extremely low (e.g.  $k < 10^{-19} \text{ m}^2$ ). The basic test system is composed of a pressure-confined rock sample connected to two closed reservoirs at its upstream and downstream ends. A pulse of pressure at the upstream boundary drives transient flow through the sample to the downstream end. The rock properties,  $k$  and  $S_s$ , can be determined by time-based recording of only one variable, the pressure change in each reservoir. Experimental error during data acquisition propagates through the data reduction process, leading to uncertainty in experimental results. In addition, unlike steady-state systems, the pressure-time curves are influenced by the compressive storage of the reservoirs and both the dimensions and properties of the sample. Thus, uncertainty in  $k$  and  $S_s$  may arise from errors in measurement of sample dimension, fluid pressure, or reservoir storages. In this study, the uncertainty in sample dimension is considered to be negligible, and reasonable error ranges in pressure and system storage measurements are considered. We first calculated pressure errors ( $P$ ) induced by the difference between assumed, or experimentally measured values of  $k$  and  $S_s$  and their true values. Based on this result, the sensitivity coefficient ( $\partial k / \partial P$  and  $\partial S_s / \partial P$ ) is theoretically  $\sim 10$  in percentage, i.e. 1% error of the pulse on average during a test cycle produces  $\sim 10\%$  uncertainty in  $k$  and  $S_s$ . The sensitivity coefficient may become larger when the ratio of sample storage to upstream reservoir storage is extremely small. We also examined the sensitivity of experimental error in measuring the storage capacity of system reservoirs to uncertainty in resulting values of  $k$  and  $S_s$ . Because the reservoirs are typically small for tight rock samples and irregular in shape due to the combination of tubing, fittings, valves, and pressure transducers, the uncertainty should be much greater than that of pressure. Our analysis reveals that 20% error in measurement of upstream storage causes  $\sim 5\text{-}15\%$  uncertainty in permeability and  $\sim 30\%$  uncertainty in specific storage, and varies linearly in this range. Our analytical model suggests that the pulse-transient method yields more accurate values of permeability than specific storage.

Final ID: V51I-03

**MASS TRANSFERS DURING SERPENTINIZATION OF OCEANIC PERIDOTITES (*Invited*)**

*M. Andreani*<sup>1</sup>; *M. Godard*<sup>2</sup>; *A. Delacour*<sup>3</sup>; *J. Escartin*<sup>4</sup>; *C. Mevel*<sup>4</sup>; *M. Muñoz*<sup>5</sup>;

1. LGL UMR5276, ENS - Univ. Lyon1, Villeurbanne, France.
2. GM UMR5243, CNRS UM2, Montpellier, France.
3. GET UMR5563, Univ. Toulouse3, Toulouse, France.
4. IPGP UMR7154, CNRS, Paris, France.
5. ISTerre UMR5275, Univ. Grenoble1, Grenoble, France.

**Body:** Mantle peridotites represent at least 20% of (ultra-)slow spread oceanic lithosphere. They are serpentinized down to several km below seafloor, and the numerous ultramafic-hosted hydrothermal systems emphasize the importance of serpentinization as a mean of chemical exchange between the mantle and the ocean. Characterizing the chemical modifications of peridotites during oceanic serpentinization and associated reactions is thus determinant to estimate the chemical fluxes near the ridges axis and the resulting input budget in subduction zones. However, these chemical exchanges are still poorly constrained. They depend on the initial chemical budget of peridotites (melting), on fluid sources (seawater or hydrothermal fluids), on sinks of elements (mineralogy), and on the operating mass transfer mechanisms, all expected to vary from one site to another.

In order to better constrain mechanisms, scale and timing of mass transfers during serpentinization of oceanic peridotites, we carried out a combined (micro)-structural, mineralogical and geochemical study of variably refertilized and serpentinized peridotites drilled at the MARK area (ODP Site 920, 23°N Mid-Atlantic Ridge).

The petrostructural study indicates that serpentinization is accompanied by abundant veining of different generations, characteristic of different mechanisms of deformation and transfer during the progressive tectonic exhumation of peridotites. Two main serpentinization stages are distinguished and rough constraints on the depth at which they occurred are provided by regional seismic velocity data. A diffusion-dominated stage occurs below ~2 km in depth. It is followed by an advection-dominated stage at shallower levels. This model is completed by a geochemical investigation of serpentinites using bulk and punctual analyses of trace elements by LA-HR-ICPMS, and iron redox state by XANES at iron K-edge. Results indicate that most samples preserve the bulk peridotite primary trace element signature except for highly mobile elements such as U (up to 10 x PM), B (4-45 ppm), As and Sb (up to 10 ppm). In situ analyses of serpentine indicate that those enrichments are strongly heterogeneous at the thin section scale. They are correlated to an increase in Fe<sup>3+</sup>/Fe<sub>Tot</sub> which follows non-linearly the local degree of serpentinization and tracks the local increase in water/rock ratio. Extensive chemical exchanges also occur for the supposedly less-mobile elements (e.g. HREE) at the thin section scale and, at the borehole scale for completely serpentinized samples: trace elements are progressively redistributed and homogenized between more and less enriched zones (e.g. Px/OI, refertilized/refractory). These observations underline the pervasive and heterogeneous nature of fluid circulation occurring at the mm scale within the forming mesh texture and within late veins at the meter scale. These results are compared to ongoing studies on the Rainbow massif that hosts an active hydrothermal field in order to characterize the effect of late and extensive hydrothermal fluid circulations on the chemical signature of oceanic serpentinites.

**On the relationship between Very-Long-Period events, bubble collapse, and eruption processes at the Lone Star Geysler, Yellowstone National Park**

*R. A. Sohn*<sup>1</sup>; *J. Vandemeulebrouck*<sup>2</sup>; *S. Hurwitz*<sup>3</sup>; *M. J. Johnston*<sup>3</sup>; *L. Karlstrom*<sup>4</sup>; *M. L. Rudolph*<sup>4</sup>; *F. Murphy*<sup>3</sup>; *C. Pontbriand*<sup>1</sup>; *G. Horning*<sup>1</sup>;

1. Geology and Geophysics, Woods Hole Oceanography Inst, Woods Hole, MA, United States.
2. Université de Savoie , Le Bourget du Lac Cedex, France.
3. U.S Geological Survey , Menlo Park, CA, United States.
4. UC Berkeley , Berkeley, CA, United States.

**Body:** Broadband seismic data acquired at the Lone Star Geysler in Yellowstone National Park over a 5-day period in September, 2010 contain Very-Long-Period (VLP) events (~2 min period) and impulsive bubble collapse events (0.25 sec duration) that are correlated with eruption/discharge cycles. Geysler 'jet' eruptions at Lone Star are fairly regular at ~3 hour (180 min) intervals, but the VLP events typically occur at ~22.5 min intervals, which is effectively a 3rd order harmonic of the jet eruption fundamental period. Bubble collapse events are impulsive with nearly monochromatic frequencies of 20-25 Hz, and the rate of these events is correlated with the VLP event cycle. These results suggest a 2-stage process model for the Lone Star eruptions, where the deep/main reservoir discharges a slug of hot water into a shallow 'chimney' every ~22.5 min, which triggers boiling and bubble collapse events as it rises and decompresses in the chimney.

Final ID: V51G-07

**Interpretation of seismic signals at Lone Star Geyser in the context of surface activity using visible and infrared video**  
*(Invited)*

*M. L. Rudolph*<sup>1</sup>; *J. Vandemeulebrouck*<sup>3</sup>; *S. Hurwitz*<sup>2</sup>; *L. Karlstrom*<sup>1</sup>; *M. J. Johnston*<sup>2</sup>; *M. Manga*<sup>1</sup>; *R. A. Sohn*<sup>4</sup>;

1. Dept of Earth and Planet Sci, University of California, Berkeley, CA, United States.
2. U.S. Geological Survey, Menlo Park, CA, United States.
3. Université de Savoie, Le Bourget du Lac, France.
4. Woods Hole Oceanographic Institute, Woods Hole, MA, United States.

**Body:** We carried out a multi-instrument geophysical study of Lone Star Geyser, Yellowstone National Park. Here, we interpret seismic signals in the context of activity at the vent as filmed using both infrared and visible light cameras. Very Long Period (VLP) seismic signals are correlated with episodes of steam discharge during periods of quiescence and with the presence of larger-than-average volumes of high-temperature steam during eruptions, favoring the interpretation of VLP pulses as characteristic of the ascent of slugs of gas through the geyser plumbing system.

**Self-potential, Ground-tilt and Infra-Red Emission Associated with Geyser Eruptions: Implications for Volcanic Monitoring.**

*M. J. Johnston*<sup>1</sup>; *S. Hurwitz*<sup>1</sup>; *R. A. Sohn*<sup>2</sup>; *J. Vandemeulebrouck*<sup>3</sup>; *L. Karlstrom*<sup>4</sup>; *M. L. Rudolph*<sup>4</sup>;

1. Earthquake Hazards, U.S. Geological Survey, Menlo Park, CA, United States.

2. Woods Hole Oceanographic Institute, Woods Hole, MA, United States.

3. Université de Savoie, Le Bourget du Lac, France.

4. U.C. Berkeley, Berkeley, CA, United States.

**Body:** Self-potential (SP), ground deformation (GD) and infrared (IR) monitoring play extremely important roles in volcano hazard assessment since they can provide valuable constraints on the depth, pressure, shape and temporal changes of both sub-surface deformation sources and surface flow patterns of hydrothermal and magmatic fluids and eruptions. However, GD in volcanic regions has usually been interpreted to result only from magma emplacement whereas recent observations of relatively rapid GD fluctuations suggest pressure transients from fluid/gas phase changes and/or hydrothermal poroelastic deformation may also contribute. Unfortunately, GD measurements that are unequivocally induced by multi-phase pressure transients with no magma involvement are rare and this has limited our ability to understand one of the major contributors to volcanic unrest. Geysers are intermittently erupting hot springs that occur when gas-rich high-temperature fluids flash to steam as a result of changing fluid/pressure/temperature conditions. These are excellent analogues to volcanoes because both systems are characterized by cyclic phenomena triggered by phase changes and fluid flow can be inferred from SP measurements. In 2009 and 2010, we documented deformation and flow in the absence of magma emplacement with measurements of SP, ground tilt (GT), IR and other parameters at “Old Faithful” and “Jones Fountain of Life” geysers in northern California and “Lone Star” geyser in Yellowstone National Park. Taking “Old Faithful” geyser as an example, the GT, SP and water outflow cycles are observed to be quasi-sinusoidal with a 4-5 minute periodicity. All are in phase except the surface eruptions. Surface eruptions occur during initial deflation about a minute after peak ground uplift and SP. The eruptions continue for about a minute with an associated small deflation/inflation pulse corresponding to first clearing then recharge of the conduit. Larger-scale deformation monitoring indicates the existence of several interacting fluid pressure sources. These observations suggest that subsurface pressure transients associated with phase changes in porous and fractured media occur at relatively shallow depths (<60m) with complex and time-variable geometry and are easily detectable with modern deformation techniques. These results are consistent with observations in volcanic regions where magma is present, and suggest that deformation techniques, together with SP and seismic monitoring, may provide an effective means for identifying and separating magmatic intrusion and subsurface hydrothermal effects.

Final ID: V52B-01

**Forward and Inverse Modeling of the seismic and electromagnetic disturbances associated with localized seismic sources in volcanic areas (*Invited*)**

*A. Revil*<sup>1, 2</sup>; *H. Mahardika*<sup>1</sup>; *A. Jardani*<sup>3</sup>;

1. Geophysics--Green Center, Colorado School of Mines, Golden, CO, United States.

2. Geophysics, ISTerre, CNRS, UMR 5559, Université de Savoie, Equipe Volcan, Bourget du Lac, France.

3. Morphodynamique Continentale et Côtière, Université de Rouen, M2C, UMR 6143, CNRS, Mont Saint Aignan, France.

**Body:** We consider a seismic source characterized by a moment tensor in a water-saturated porous material with piece-wise constant seismic velocities corresponding to different geological units. We have developed a finite element code to compute the seismograms, the electrograms and the magnetograms associated with the source, the conversion of the mechanical energy to electromagnetic energy at the position of heterogeneities and the co-seismic signals traveling at the same speed than the seismic waves. In our model, the electromagnetic energy is generated through the electrokinetic coupling in porous materials. This coupling is related to the relative displacement between the pore water and the mineral grains coated by the electrical double layer. We show that in the case of a noisy environment, the electromagnetic information is complementary to the seismic information to recover the position of the source and to invert the moment tensor, which in turn provides information on the stress state of the volcano.

**Magma replenishment and volcanic unrest inferred from the analysis of VT micro-seismicity and seismic velocity changes at Piton de la Fournaise Volcano**

*F. Brenguier*<sup>1, 2</sup>; *E. Rivemale*<sup>2</sup>; *D. S. Clarke*<sup>2</sup>; *A. Schmid*<sup>3</sup>; *J. Got*<sup>4</sup>; *J. Battaglia*<sup>5</sup>; *B. Taisne*<sup>2</sup>; *T. Staudacher*<sup>1</sup>; *A. Peltier*<sup>2</sup>; *N. M. Shapiro*<sup>2</sup>; *S. Tait*<sup>2</sup>; *V. Ferrazzini*<sup>1</sup>; *A. Di Muro*<sup>1</sup>;

1. P. de la Fournaise Volc. Obs., Institut de Physique du Globe de Paris, La Plaine Des Cafres, France.

2. Institut de Physique du Globe de Paris, Paris, France.

3. ISTERre, Grenoble, France.

4. ISTERre, Chambéry, France.

5. LMV, Clermont-Ferrand, France.

**Body:** Piton de la Fournaise volcano (PdF) is among the most active basaltic volcanoes worldwide with more than one eruption per year on average. Also, PdF is densely instrumented with short-period and broad-band seismometers as well as with GPS receivers. Continuous seismic waveforms are available from 1999. Piton de la Fournaise volcano has a moderate inter-eruptive seismic activity with an average of five detected Volcano-Tectonic (VT) earthquakes per day with magnitudes ranging from 0.5 to 3.5. These earthquakes are shallow and located about 2.5 kilometers beneath the edifice surface. Volcanic unrest is captured on average a few weeks before eruptions by measurements of increased VT seismicity rate, inflation of the edifice summit, and decreased seismic velocities from correlations of seismic noise. Eruptions are usually preceded by seismic swarms of VT earthquakes. Recently, almost 50 % of seismic swarms were not followed by eruptions. Within this work, we aim to gather results from different groups of the UnderVolc research project in order to better understand the processes of deep magma transfer, volcanic unrest, and pre-eruptive magma transport initiation. Among our results, we show that the period 1999–2003 was characterized by a long-term increase of VT seismicity rate coupled with a long-term decrease of seismic velocities. These observations could indicate a long-term replenishment of the magma storage area. The relocation of ten years of inter-eruptive micro-seismicity shows a narrow (~300 m long) sub-vertical fault zone thus indicating a conduit rather than an extended magma reservoir as the shallow magma feeder system. Also, we focus on the processes of short-term volcanic unrest and prove that magma intrusions within the edifice leading to eruptions activate specific VT earthquakes that are distinct from magma intrusions that do not lead to eruptions. We thus propose that, among the different pathways of magma transport within the edifice, only one will allow magma to reach the edifice summit. Moreover, we have identified transient seismic velocity changes lasting a few weeks that could be associated with unreported lateral magma intrusions not leading to eruptions. The clustering of pre-eruptive micro-seismicity between mid 1999–2003 shows that seismic events repeat over successive seismic swarms and suggests that the magma pathway is spatially separated from the seismic faults. Also, the inversion for focal mechanisms shows dominant sub-horizontal P-axes indicating that part of the pre-eruptive micro-seismicity is due to the horizontal compressive stress induced by magma injection. Finally, the analysis of long-term GPS data recorded on the edifice flank shows a constant lateral displacement rate of 3.5 cm/year. More work will be needed in order to infer the possible mutual interactions between magma unrest and transport and the large-scale deformation of the edifice flank.

Final ID: V53A-2582

**Periodic flow instabilities during Lone Star Geyser (YNP) eruptions, as deduced from acoustic measurements.**

*J. Vandemeulebrouck*<sup>1</sup>; *S. Hurwitz*<sup>2</sup>; *M. J. Johnston*<sup>2</sup>; *M. L. Rudolph*<sup>3</sup>; *L. Karlstrom*<sup>3</sup>; *R. A. Sohn*<sup>4</sup>; *F. Murphy*<sup>2</sup>; *D. K. McPhee*<sup>2</sup>; *J. M. Glen*<sup>2</sup>; *S. A. Soule*<sup>4</sup>; *C. M. Meertens*<sup>5</sup>;

1. ISTERre, Universite de Savoie, Chambéry, France.
2. US Geological Survey, Menlo Park, CA, United States.
3. Dept Earth And Planetary Science, UC Berkeley, Berkeley, CA, United States.
4. WHOI, Woods Hole, MA, United States.
5. Unavco, Boulder, CO, United States.

**Body:** We performed continuous acoustic measurements during four days at Lone Star Geyser, Yellowstone National Park, USA. The microphone was located at 10 meters from the geyser's cone, and the acoustic signal was sampled at 1000 Hz. The 3-hour-long eruptive cycle at Lone Star Geyser contains several water fountaining episodes followed by the main eruption, which generally lasts 25 minutes. During the 30 main eruptions that we studied, the acoustic signal patterns are very similar, and indicate the flow is unstable and clearly follows a pulsating regime. The period of the acoustic pulses drastically increases during the liquid to steam transition in the flow. This abrupt change in the flow regime corresponds to the start of the ground deflation recorded by tiltmeters, and could be due to a transition from hydro-static to vapor-static conditions in the vent.

**Direct Measurement of the Volume of Liquid Water Emitted During Eruptions of Lone Star Geyser, Yellowstone National Park, Wyoming**

*F. Murphy*<sup>1</sup>; *S. Hurwitz*<sup>1</sup>; *M. J. Johnston*<sup>1</sup>; *J. Vandemeulebrouck*<sup>2</sup>; *C. Pontbriand*<sup>3</sup>; *R. A. Sohn*<sup>3</sup>; *L. Karlstrom*<sup>4</sup>; *M. L. Rudolph*<sup>4</sup>;

1. USGS, Menlo Park, CA, United States.
2. Université de Savoie, Grenoble, France.
3. Woods Hole Oceanographic Institute, Woods Hole, MA, United States.
4. U.C. Berkeley, Berkeley, CA, United States.

**Body:** In September, 2010 a comprehensive series of instrumental observations was carried out at Lone Star Geyser in Yellowstone National Park to measure changes in the geyser and its surroundings during eruptions. That project included measurements of flow in the streams that drain the geyser area. Three small streams convey liquid water from the geyser and many of the surrounding hot springs to the Firehole River, about 75 m south of the geyser cone. We developed rating curves for two of these streams by measuring channel cross-sections and timing floating markers (using stopwatches and video recordings) while simultaneously recording stream depth at two-second intervals at two locations using pressure transducers and dataloggers. We estimated the flow in the third (ungaged) stream to be 0.15 of the flow in the easternmost stream, with which it shares a source area and part of its channel. The eruption cycle takes about 3 hours, and a total of nine eruption cycles were observed. During these 3-hour cycles the geyser and the nearby hot springs deliver a total of between 15 and 28 m<sup>3</sup> of water to the Firehole River. During the 10-20 minutes of the main phase of an eruption, the geyser delivered between 8 and 11 m<sup>3</sup> of water to the three streams. The volume of water emitted during eruptions appears to display a significant diurnal variation which strongly correlates with air temperature, with significantly more flow during early afternoon hours. There were also significant variations in the distribution of flow between the different channels. Our calculations suggest that losses due to evaporation along the flow channels are negligible, and losses due to infiltration appear to be small. The calculated volumes of water discharge do not account for the volume of erupted steam or evaporation of liquid water from the jet. Steam discharge will be assessed using image analysis of high speed video. The calculated volumes provide accurate and important constraint for models of geyser jet dynamics, energetics, and mass balance.

**A Multi-Method Experiment to Investigate Geyser Dynamics: Lone Star Geyser, Yellowstone National Park**

*S. Hurwitz*<sup>1</sup>; *J. Vandemeulebrouck*<sup>2</sup>; *M. J. Johnston*<sup>1</sup>; *R. A. Sohn*<sup>3</sup>; *L. Karlstrom*<sup>4</sup>; *M. L. Rudolph*<sup>4</sup>; *F. Murphy*<sup>1</sup>; *D. K. McPhee*<sup>1</sup>; *J. M. Glen*<sup>1</sup>; *S. A. Soule*<sup>3</sup>; *C. Pontbriand*<sup>3</sup>; *C. M. Meertens*<sup>5</sup>;

1. U.S. Geological Survey, Menlo Park, CA, United States.
2. ISTERre, Université de Savoie , Le Bourget du Lac Cedex, France.
3. Woods Hole Oceanographic Institution, Woods Hole, MA, United States.
4. Dept Earth and Planetary Science, UC Berkeley, Berkeley, CA, United States.
5. UNAVCO, Boulder, CO, United States.

**Body:** Geysers are intermittently discharging hot springs that are driven by steam and non-condensable gas. They provide unique opportunities to study multiphase eruption processes and the geophysical signals they induce. In September 2010 we carried out a four-day experiment at Lone Star Geyser in Yellowstone National Park. The geyser is located about 5 km SSE of Old Faithful Geyser and 75 m north of the Upper Firehole River. Lone Star is a cone geyser that was selected for the experiment because it is isolated from other geysers, its eruptions are vigorous and voluminous, and its eruption intervals are relatively constant and predictable, occurring approximately every 3 hours. We made measurements during 32 eruption cycles using a suite of instruments including a broadband seismometer, 2 microphones, 5 platform tiltmeters, 3 collimating InfraRed sensors, 2 gravimeters, 2 self-potential sensors, 2 Light Detection And Ranging (LiDAR) scanners, a Forward Looking InfraRed (FLIR) camera, high-speed video cameras, and stream gauging. We also integrated meteorological data from nearby weather stations. The large dataset acquired during the experiment allows for the detection of a myriad of processes in the subsurface and in the erupting column at many different frequencies. The analyzed data yield new insights on multiphase eruptive processes that have implications for understanding self-organized, intermittent processes in nature that result from phase separation and localized input of energy and mass. The geophysical signals recorded during the experiment allow comparison with signals recorded in more complex volcanic systems where gas-driven and magma-driven processes are often hard to distinguish.

**Volcano-tectonic earthquake source mechanisms during magma ascent at Piton de la Fournaise volcano.**

*A. Schmid*<sup>1</sup>; *P. Lemarchand*<sup>3</sup>; *F. Brenguier*<sup>2</sup>; *O. Coutant*<sup>1</sup>; *A. Maggi*<sup>3</sup>;

1. ISTERre, St Martin D'Herès, France.

2. IPGP, Paris, France.

3. IPGS, Strasbourg, France.

**Body:** In this study, we aim at determining the focal mechanisms of the volcano-tectonic (VT) seismicity of Piton de la Fournaise volcano, in order to get information on any permanent or transient stress trends inside the volcanic edifice, and to test if the evolution of the stress can be related to eruption occurrences.

The VT seismicity usually recorded on volcanoes shows small magnitudes ( $\text{Mag} < 3$ ) and short-period waveforms. It is difficult to assess the source parameters of those waves with classical tools, since they are very sensitive to crustal scattering, particularly in volcanic contexts showing complex crustal structures. Our crustal models are not precise enough to take into account the small heterogeneities.

Here we propose and apply a technique for inverting short period (1-10Hz) waveforms amplitudes of small VT events ( $\text{Mag} < 3$ ) recorded on Piton de la Fournaise volcano, in order to determine their focal mechanisms.  $\text{Mag} > 2.5$  events with well-constrained source mechanisms (from polarity inversion) are used to calibrate the "unmodeled" structural effects. This calibration is made possible since multiplets (similar waveforms) have been recorded including different size of events and spread over long periods, accounting for the stability of the propagation properties. Following Tan and Don Helmberger (2007), we define amplitude amplification factors AAF as the ratio between recorded amplitudes and analytical computation of expected amplitudes from radiation patterns. Those factors (determined on the  $\text{mag} > 2.5$  events) are then used as a calibration to inverse recorded amplitudes on smaller events.

We then use a grid-search approach to determine source mechanisms by minimizing the misfit error between real and synthetic amplitudes. We applied this technique on two datasets extracted from the VT seismicity of Piton de la Fournaise volcano: i) a selection of the larger events ( $\text{mag} > 2.5$ ) over 2009-2011, and ii) the pre-eruptive swarm of the October 2010 eruption (more than 700 picked events).

This approach allowed us to propose a new insight on the Piton de la Fournaise seismicity's source mechanisms. The observed main P-axes set up some preferential stress axes to be related with magmatic activity. The frequent occurrence of similar source mechanisms allowed us to identify families of events accounting for different source locations. The expression of those identified families of VT events might be considered as pre-eruptive information.

**Muon tomography of the Soufrière of Guadeloupe (Lesser Antilles): Comparison with other geophysical imaging methods and assessment of volcanic risks.**

*B. Taisne*<sup>1</sup>; *D. Gibert*<sup>1</sup>; *N. Lesparre*<sup>1</sup>; *J. Marteau*<sup>2</sup>; *F. Nicollin*<sup>3</sup>; *O. Coutant*<sup>4</sup>;

1. Institut de Physique du Globe de Paris (UMR CNRS/INSU 7154), Sorbonne Paris Cité, Paris, France.

2. Institut de Physique Nucléaire de Lyon (UMR CNRS/IN2P2 5822), Lyon, France.

3. Géosciences Rennes (UMR CNRS/INSU 6118), Rennes, France.

4. Institut des Sciences de la Terre (UMR CNRS/INSU 5275, IRD UR 219), Grenoble, France.

**Body:** Density tomography of rock with muons of cosmic origin measures the attenuation of the flux of particles crossing the object of interest to derive its opacity, i.e. the quantity of matter encountered by the particles along their trajectories. Recent progress in micro-electronics and particle detectors make field measurement possible and muon density tomography is gaining a growing interest (e.g. Tanaka et al., 2010; Gibert et al., 2010). We have constructed field telescopes based on the detectors of the OPERA experiment devoted to study neutrino oscillation (Lesparre et al., 2011a). Each telescope may be equipped with a variable number of detection matrices with 256 pixels. The spatial resolution is adaptable and is typically of about 20 meters (Lesparre et al., 2010). The telescopes are portable autonomous devices able to operate in harsh field conditions encountered on tropical volcanoes. The total power consumption is less than 40W, and an Ethernet link allows data downloading and remote control of the electronic devices and on-board computers. Larger high-resolution telescopes are under construction.

The instruments have been successfully tested on the Etna and Soufrière of Guadeloupe volcanoes. A telescope is operating continuously since Summer 2010. Muon radiographies of the Soufrière lava dome reveal its very heterogeneous density structure produced by an intense hydrothermal circulation of acid fluids which alters its mechanical integrity leading to a high risk level of destabilisation. Small-size features are visible on the images and provide precious informations on the structure of the upper hydrothermal systems. Joined interpretation with other geophysical data available on the Soufrière – seismic tomography, electrical resistivity tomography, gravity data – is presented and discussed. Density muon tomography of the internal structure of volcanoes like the Soufrière brings important informations for the hazard evaluation and is particularly adapted to brought constraints on flank destabilization and hydrothermal circulation models.

Tanaka et al., Three dimensional computational axial tomography scan of a volcano with cosmic ray muon radiography, *J. Geophys. Res.*, 115, B12332, doi:10.1029/2010JB007677, 2010.

Gibert et al., Muon Tomography: Plans for Observations in the Lesser Antilles, *Earth Planets and Space*, Vol. 52, 153-165, doi: 10.5047/eps.2009.07.003, 2010.

Lesparre et al., Geophysical muon imaging: feasibility and limits, *Geophysical Journal International*, Vol. 183, 1348-1361, doi: 10.1111/j.1365-246X.2010.04790.x, 2010.

Lesparre et al., Design and Operation of a Field Telescope for Cosmic Ray Geophysical Tomography, *Nuclear Instruments and Methods in Physics Research A*, to appear, 2011a.

Lesparre et al., Bayesian Dual Inversion of Experimental Telescope Acceptance and Integrated Flux for Geophysical Muon Tomography, *Geophysical Journal International*, to appear, 2011b.

**URL:** <http://www.ipgp.fr/~gibert/>

Final ID: U53E-03

**Climate effects on volcanism: Influence of ice load variations on magma storage zones with application to Icelandic volcanoes. (Invited)**

*F. Albino*<sup>1</sup>; *V. Pinel*<sup>2</sup>; *F. Sigmundsson*<sup>1</sup>;

1. Nordic Volcanological Center, Institute of Earth Sciences, University of Iceland, Reykjavik, Iceland.

2. ISTerre, IRD, Universite de Savoie, Le Bourget Du Lac, France.

**Body:** Correlations between deglaciation periods and eruptive activity in the past have been strongly suggested, especially in Iceland, where the end of the last glaciation was characterised by a large pulse in volcanic production. Present-day reduction in ice load on subglacial volcanoes due to global warming is modifying pressure conditions in magmatic systems with a potential to influence magma production as well as shallow storage. Here, we model stress induced by variation in surface loads and evaluate how the resulting pressure conditions can modulate magmatic activity. We focus on the effect on shallow storage zones and show that ice loading can modify their failure conditions in a manner that depends critically on ice retreat timing and spatial distribution, the shape and depth of magma chambers as well the compressibility of the magma. We study in particular two subglacial volcanoes in Iceland: the Katla volcano under the Mýrdalsjökull ice cap and Grímsvötn at the Vatnajökull ice cap. Numerical calculations have been carried out in axisymmetric geometry for elliptical magma chambers. An elastic model is first used to evaluate the effects of the annual load cycle, due to seasonal variation of ice mass, which indicates an annual modulation of failure conditions on magma chambers at subglacial volcanoes. Our model predicts that, in case of a spherical or horizontally elongated magma chamber, eruptions are more likely when the seasonal snow cover is smallest. This triggering effect is small, around few kPa, but appears consistent with the fact that all the nine last major historical eruptions of Katla volcano occurred in period from May – October when the annual snow load is minimum. Viscous effects are then introduced to evaluate the influence of long term ice thinning on the shallow magma storage zones.

Final ID: GP54A-06

### Pyrrhotite remagnetizations in Himalayan rocks

*E. Appel*<sup>1</sup>; *C. Crouzet*<sup>2</sup>; *E. Schill*<sup>3</sup>;

1. Department of Geosciences, University Tübingen, Tübingen, Germany.
2. Institut des Sciences de la Terre, Université de Savoie, Le Bourget du Lac, France.
3. Institut de Géologie et d'Hydrogéologie, Université de Neuchâtel, Neuchâtel, Switzerland.

**Body:** Pyrrhotite remagnetization is a widespread phenomenon in the Himalaya. Throughout the last two decades a large data set has been acquired and successfully interpreted, in particular from low-grade metamorphic rock of the Tethyan Sedimentary Series (TSS). The nature of the remanence is a TRM when the peak metamorphic temperature  $T_{max}$  exceeded the Curie temperature ( $T_c \approx 325^\circ\text{C}$ ) of pyrrhotite and in this case its remanence age can be related to the last metamorphic cooling. In case of  $T_{max}$  did not reach  $T_c$  a CRM, TCRM or (p)TRM are possible. Cooling ages show a systematic trend of ~50-20 Ma from the western to the eastern Himalaya. The pyrrhotite remagnetizations postdate the main Himalayan folding and record late orogenic rotations and long-wavelength tiltings around vertical and horizontal axes, which can be related to large-scale deformation such as rotational shortening between the Indian and Asian plates, oroclinal bending, eastward extrusion of the Tibetan Plateau, as well as to meso-scale effects due to crustal doming. Consistent pyrrhotite remanences are especially typical for low-grade marly limestones in the TSS, but were also found in medium-grade Lesser Himalayan rocks, in the high-grade Higher Himalayan Crystalline, and surprisingly in weakly metamorphic diorite dykes of SE Tibet. In the dykes sulphur migration from the host rocks (flysch) during metamorphic conditions is suspected as the cause of pyrrhotite formation. While the pyrrhotite remanences are predominantly very stable in low-grade metamorphic meta-sediments they are often less clear in higher-grade rocks probably due to growth of larger grains and therefore softer magnetic behaviour. Inconsistent results, mainly observed in higher-grade rocks, could be explained by remanence acquisition during cooling while still ductile deformation was prevailing. The possible influence of the strong magnetocrystalline anisotropy of pyrrhotite on remanence directions was tested by ARM experiments. The resulting ARM directions and the direction of the ARM imparting direct field do not reveal a significant deviation.